

SCIENTIFIC REPORTS



OPEN

Antitumor properties of Coenzyme Q₀ against human ovarian carcinoma cells *via* induction of ROS-mediated apoptosis and cytoprotective autophagy

You-Cheng Hseu^{1,2}, Tai-Jung Tsai³, Mallikarjuna Korivi³, Jer-Yuh Liu⁴, Hui-Jye Chen⁵, Chung-Ming Lin⁶, Yi-Chun Shen³ & Hsin-Ling Yang³

Coenzyme Q₀ (CoQ₀, 2,3-dimethoxy-5-methyl-1,4-benzoquinone) has been reported to exert anticancer properties against human breast/lung cancer cells. This study investigated the *in vitro* and *in vivo* anticancer properties of CoQ₀ on human ovarian carcinoma (SKOV-3) cells and xenografted nude mice, and revealed the underlying molecular mechanism. CoQ₀ induced G₂/M arrest through downregulation of cyclin B1/A and CDK1/K2 expressions. CoQ₀-induced autophagy as a survival mechanism was evidenced by increased accumulation of LC3-II, GFP-LC3 puncta, AVOs formation and Beclin-1/Bcl-2 dysregulation. Increased TUNEL-positive cells and Annexin-V/PI stained cells indicated CoQ₀-induced late apoptosis. Both mitochondrial (caspase-3, PARP and Bax/Bcl-2 dysregulation) and ER stress (caspase-12 and Hsp70) signals are involved in execution of apoptosis. Interestingly, CoQ₀-induced apoptosis/autophagy is associated with suppression of HER-2/*neu* and PI₃K/AKT signalling cascades. CoQ₀ triggered intracellular ROS production, whereas antioxidant *N*-acetylcysteine prevented CoQ₀-induced apoptosis, but not autophagy. Inhibition of apoptosis by Z-VAD-FMK suppressed CoQ₀-induced autophagy (diminished LC3-II/AVOs), indicates CoQ₀-induced apoptosis led to evoke autophagy. Contrary, inhibition of autophagy by 3-MA/CQ potentiated CoQ₀-induced apoptosis (increased DNA fragmentation/PARP cleavage). Furthermore, CoQ₀ treatment to SKOV-3 xenografted nude mice reduced tumor incidence and burden. Histopathological analyses confirmed that CoQ₀ modulated xenografted tumor progression by apoptosis induction. Our findings emphasize that CoQ₀ triggered ROS-mediated apoptosis and cytoprotective autophagy.

Cancer is one of the pathological scenarios where apoptosis is inactivated, resulting in accumulation of malignant cells that will not die. Ovarian cancer is the seventh most common cancer in women worldwide, which accounts for nearly 4% of all new cases of cancer in women. This lethal malignancy usually diagnosed at later stage with a 5 years survival rate of below 30%. Since most of the ovarian cancer cases are diagnosed after wide spreading of tumors within the peritoneal cavity, it is restraining the effectiveness of chemotherapy, and associated death is believed to be therapy-resistant metastasis^{1,2}. The prognosis is usually poor for ovarian cancer patients, because the disease reaching an advanced stage before it is discovered³. Despite overall declining death rates for cervical and uterus cancers, the annual report of ovarian cancer mortality has risen by 250% since 1930⁴. Primary cytoreductive surgery followed by chemotherapy with anticancer agents is the standard treatment regimen for patients

¹Department of Cosmeceutics, College of Biopharmaceutical and Food Sciences, China Medical University, Taichung, 40402, Taiwan. ²Department of Health and Nutrition Biotechnology, Asia University, Taichung, 41354, Taiwan. ³Institute of Nutrition, College of Biopharmaceutical and Food Sciences, China Medical University, Taichung, 40402, Taiwan. ⁴Graduate Institute of Cancer Biology, China Medical University, Taichung, 40402, Taiwan. ⁵Graduate Institute of Basic Medical Science, China Medical University, Taichung, 402, Taiwan. ⁶Department of Biotechnology, Ming Chuan University, Taoyuan, 333, Taiwan. Correspondence and requests for materials should be addressed to H.-L.Y. (email: hlyang@mail.cmu.edu.tw)

with ovarian cancer, which improved survivals. Nevertheless, most of the patients with advanced cancer will eventually relapse and die of their cancer^{2,5}. A preliminary study showed improved efficacy of chemotherapy and normalized cancer biomarkers following a high-dose of antioxidant (containing coenzyme Q₁₀) treatment with chemotherapy in patients with advanced ovarian cancer⁶. Management of ovarian cancers is still in high demand for effective therapy without adverse effects caused by the therapeutic agents.

Despite being the cause of problem, apoptosis or programmed cell death plays an important role in treatment of cancers, as it is a popular target of many therapeutic strategies. Mounting evidence revealed that induction of apoptosis by chemical substances or pro-apoptotic agents eventually controlled the spreading of cancer^{7–9}. Apoptotic signals are reported to be triggered by several cellular events, including excessive production of reactive oxygen species (ROS), mitochondrial dysfunction and ER stress^{8,10,11}. The apoptotic signals either intrinsic or extrinsic cascades lead to activate the caspases, a class of cysteine proteases that cleave different substrates and ultimately leading to cell dismantling and DNA fragmentation^{12,13}. In apoptosis, caspases can also cleave Beclin-1, an autophagic protein, and inhibit its pro-autophagic activity. Autophagy, a process of programmed cell survival or an adaptive response is activated during periods of cellular distress and extinguished during the cell-cycle¹⁴. At the molecular level, autophagy is regulated by a battery of signals, such as microtubule-associated protein light chain-3 (LC3), mammalian target of rapamycin (mTOR), autophagy-related protein 7 (ATG7) and Beclin-1. In addition, formation of acidic vesicular organelles (AVOs) is a hallmark of autophagy^{15,16}. Some anti-cancer agents that can induce apoptosis also stimulate autophagy as a death mechanism¹⁷. Recent developments in cancer research suggest that autophagy could be an additional target for adjuvant anticancer treatment, and inhibition of autophagy could strengthen the therapeutic efficacy of cancer treatment^{18,19}. However, whether autophagy promotes or inhibits cancer cell death in response to cellular stress is controversial. Indeed, there is a crosstalk between autophagy and apoptosis as they share common stimuli and signalling pathways^{14,20,21}. Thus, understanding of the complex relation between apoptosis and autophagy in cancer therapy could enhance the treatment effectiveness.

Coenzyme Q (CoQ) is a well-known biomolecules comprised of a quinone nucleus and a hydrophobic side chain containing variable number of *trans*-isoprenoid units. CoQ₁₀ is the major naturally occurring form of CoQ that containing 10 isoprenoid units, while CoQ₀ is the novel analog without isoprenoid side chains²². Various CoQ analogs or ubiquinone (Ub) have been reported to either increase or decrease the production of ROS, and involved in opening/closing of mitochondrial permeability transition pore (PTP), which relies on cellular context^{8,23}. CoQ analogs with shorter isoprenoid side chains (CoQ₂ and CoQ₄) reported to induce apoptosis in mutated BALL-1 cells, but not longer isoprenoid chains (CoQ₆ and CoQ₁₀)²⁴. Among various CoQ analogs (Ub₂ and Ub₁₀), CoQ₀, a redox active compound profoundly triggered the ROS production in Clone-9 cells, induced PTP opening in cancerous rat liver MH1C1 cells and promote cell death²³. CoQ₀ has been shown as a potent cytotoxic compound towards human breast cancer cells by induction of apoptosis and cell-cycle arrest²⁵. Our recent findings showed anti-angiogenic property of CoQ₀ in stimulated human endothelial cells²⁶.

Previously, we have shown the potent anticancer properties of *Antrodia camphorata* against human ovarian cancers via induction of apoptosis and cell-cycle arrest²⁷. Several studies showed free radical scavenging or anti-oxidant activity^{28,29} and anticancer properties of *Antrodia camphorata*, a well-known medicinal mushroom in Taiwan^{30–32}. However, those studies are limited to claim the responsible bioactive compounds, and yet no study to demonstrate the anticancer properties of CoQ₀, a key ingredient in *Antrodia camphorata*. In this study, we used CoQ₀ that is isolated from *Antrodia camphorata*, and investigated its anticancer potentials in human ovarian cancer (SKOV-3) cells and xenografted nude mice. To distinguish the underlying molecular mechanisms, the effect of CoQ₀ on ROS production; and the role of ROS on cancer cell survival, apoptosis and autophagy were examined by determining the key molecules involved in regulation of apoptosis and autophagy in SKOV-3 cells.

Results

CoQ₀ inhibits viability and growth of human ovarian carcinoma cells. Prior to explore its anti-cancer properties, we examined the cytotoxic effects of CoQ₀ on human ovarian carcinoma cell lines (SKOV-3, A2780 and A2870/CP70) and normal ovarian surface epithelial (IOSE) cells. Treatment of cells with increasing concentrations of CoQ₀ (0–40 μM, 24 h) dose-dependently decreased viability of SKOV-3, A2780 and A2870/CP70 cells with the IC₅₀ values of 26.6, 27.3 and 28.4 μM, respectively (Fig. 1B–D). The cytotoxic concentration of CoQ₀ on normal IOSE cell lines is >40 μM (Fig. 1E). Inhibition of SKOV-3 cell viability with CoQ₀ was prominent event at 20 μM concentration compared to A2780 and A2870/CP70 cell lines (Fig. 1B). Higher concentration of CoQ₀ caused severe abrupt morphological changes, which were represented by cell shrinkage and decreased density of SKOV-3 cells (Fig. 1F). We assume that the cytotoxic effect of CoQ₀ may be due to the induction of cell-cycle arrest.

CoQ₀ induces G₂/M cell-cycle arrest and reduces cell-cycle proteins in SKOV-3 cells. To address whether CoQ₀ induces cell-cycle arrest in SKOV-3 cells, we measured the distribution of cells (%) in different phases of cell-cycle following CoQ₀ treatment (0–30 μM, 24 h). Flow cytometry data showed that CoQ₀ resulted in a progressive and sustained accumulation of cells in G₂/M phase, while cells in G₁ phase were gradually decreased in a dose-dependent fashion. The accumulation of cells in G₂/M phase is ~30.5% with 30 μM CoQ₀, whereas cells in G₂/M phase are only 8.9% without CoQ₀ treatment (Fig. 1G). Concurrently, the expressions of cell-cycle regulatory proteins, including cyclin B1, cyclin dependent kinase 1 (CDK1), cyclin A and CDK2 were dose-dependently decreased with CoQ₀ (Fig. 1H). These results explain that CoQ₀ considerably inhibited ovarian cancer (SKOV-3) cell proliferation through induction of G₂/M cell-cycle arrest and reduction of cell-cycle regulatory proteins.

CoQ₀ triggers intracellular ROS levels to promote SKOV-3 cell death. Excessive generation of ROS by oxidants/chemical substances is reported to potentiate cancer cell death *via* apoptosis or autophagy

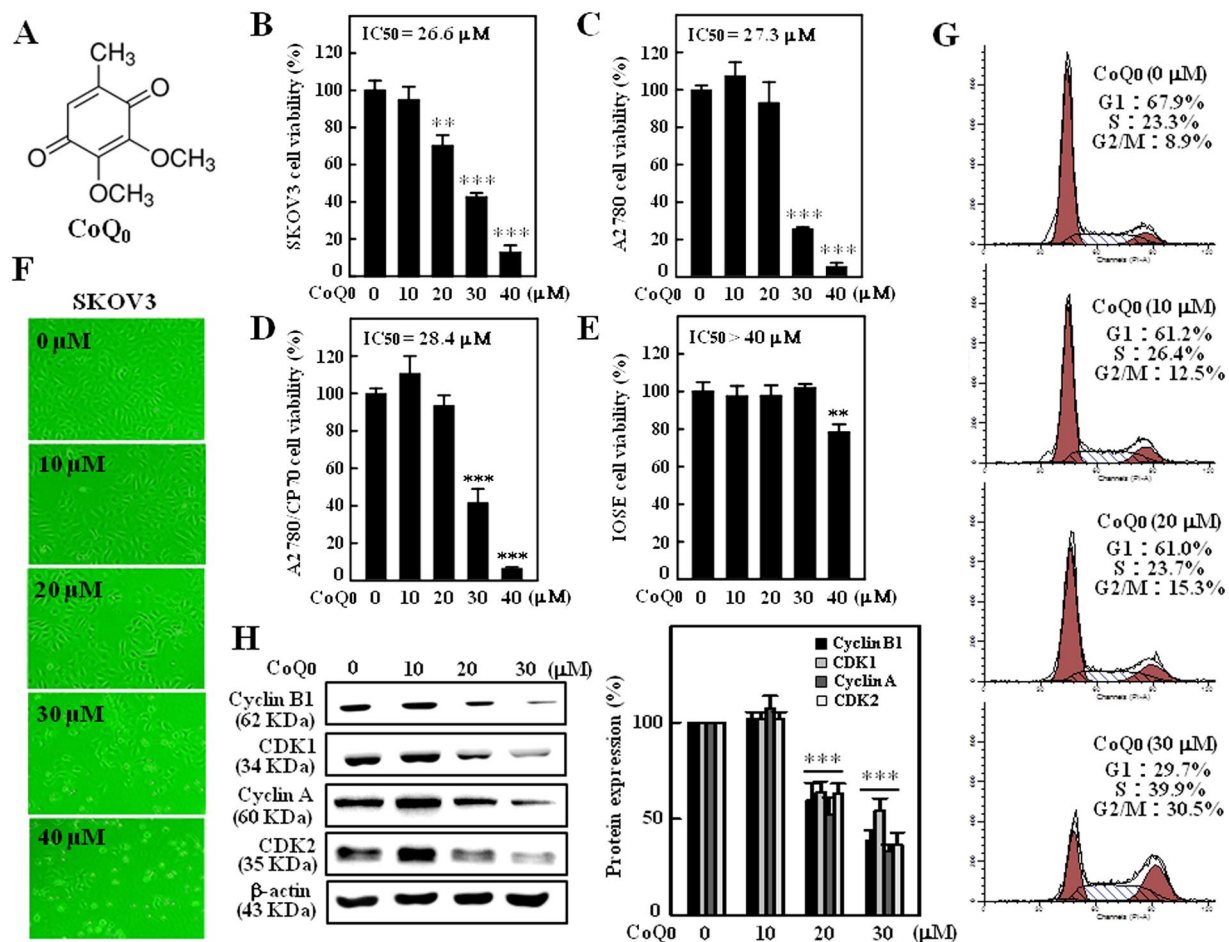


Figure 1. CoQ₀ inhibits growth of human ovarian carcinoma cells and induces G2/M cell-cycle arrest in SKOV-3 cells. (A) Structure of CoQ₀. (B–D) Human ovarian carcinoma (SKOV-3, A2780 and A2780/CP-70) and (E) human ovarian surface epithelial (IOSE) cells were treated with increasing concentrations of CoQ₀ (0–40 μM) for 24 h. Cell viability was determined using MTT assay. (F) Morphological changes in CoQ₀-treated (0–40 μM, 24 h) SKOV-3 cells were examined by phase-contrast microscope (200 × magnification). (G) SKOV-3 cells were treated with CoQ₀ (0–30 μM) for 24 h, stained with PI and analyzed for cell-cycle phase using flow cytometry. The cellular distributions (percentage) in different phases of cell-cycle (G1, S and G2/M) were determined after CoQ₀ treatment. Flow cytometry images shown here are from one representative analysis that was repeated three times with similar results. (H) SKOV-3 cells were treated with CoQ₀ (0–30 μM) for 24 h, and cell-cycle regulatory proteins, cyclin B1, CDK1, cyclin A and CDK2 were examined using Western blot. Relative changes in protein intensities were quantified by commercially available software, and presented as histogram, control being as 1-fold. Results expressed as mean ± SD of three independent assays (n = 3), and significant at ***p* < 0.01; ****p* < 0.001 compared with untreated control cells.

mechanisms³³. We found treatment of SKOV-3 cells with CoQ₀ (30 μM) for 0–30 min remarkably increased the intracellular ROS levels. Especially, ROS levels at 15 min following CoQ₀ treatment were significantly higher (~38 fold) than the control, as evidenced by increased dichlorofluorescein (DCF) (Fig. 2A and B). Interestingly, cells incubated with ROS inhibitor (N-acetylcysteine [NAC], 2 mM) 1 h prior to CoQ₀ treatment (0–30 μM, 15 min) substantially inhibited the ROS production (Fig. 2C and D). We further demonstrated that NAC pretreatment completely reversed the CoQ₀-induced death of SKOV-3 cells (Fig. 2E). These findings suggest that CoQ₀ triggered intracellular ROS generation and that are possibly contribute to death of SKOV-3 cells.

CoQ₀ promotes LC3 accumulation and AVOs formation in SKOV-3 cells. LC3, a promising autophagy marker exists in LC3–I (cytosolic) and LC3–II (membrane bound) forms. The conversion of LC3–I to LC3–II or accumulation of LC3–II is correlated with the extent of autophagosome formation or increased numbers of AVOs in cells^{15, 16}. To address whether CoQ₀ could induce autophagy, we measured the conversion of LC3–I to LC3–II and AVOs formation following CoQ₀ treatment (0–30 μM). As presented in Fig. 3A, CoQ₀ dose-dependently increased the LC3–II accumulation in SKOV-3 cells. The sequential effect of CoQ₀ on AVOs formation was measured *via* fluorescence microscope using acridine orange (AO) stain. Arrows on images clearly indicating the increased appearance of AVOs (red fluorescence), following CoQ₀ treatment (Fig. 3B). The high

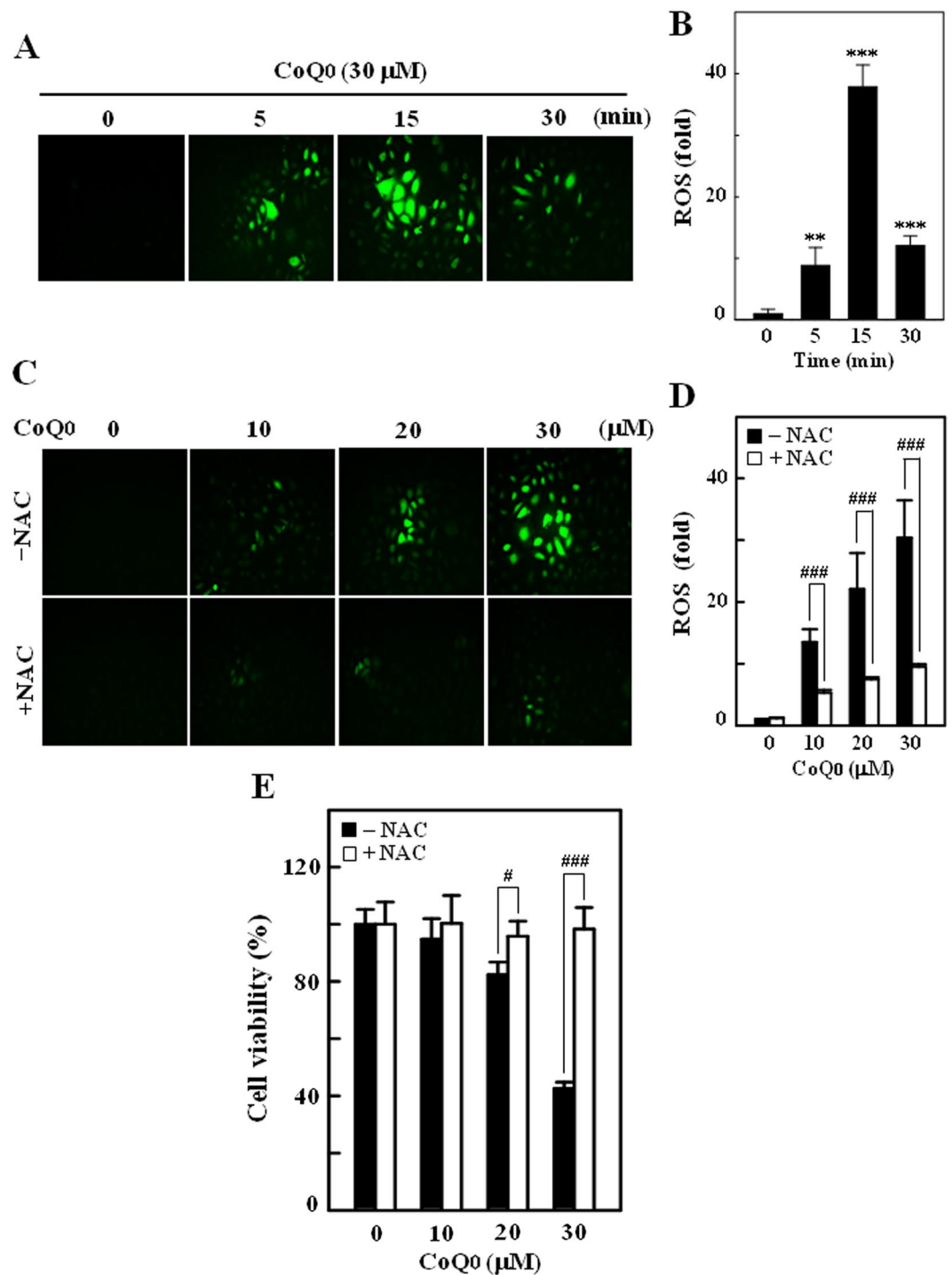


Figure 2. CoQ₀ induces intracellular ROS generation in SKOV-3 cells. (A) Cells were treated with CoQ₀ (30 μM) for 0–30 min and generation of intracellular ROS were measured using fluorescent microscopy (200 × magnification). The non fluorescent probe DCFH₂-DA reacts with cellular ROS and metabolized into fluorescent DCF. (B) The fluorescence intensity of DCF-stained cells, represent the levels of ROS was quantified by Olympus Soft Imaging Solution, and presented as histogram. Results are significant at $**p < 0.01$; $***p < 0.001$ compared to time 0 min. (C) Cells were treated with CoQ₀ (10–30 μM) for 15 min, and ROS generation was measured in the presence or absence of ROS inhibitor (2 mM NAC, 1 h prior to CoQ₀). The levels of intracellular ROS were indicated by strong or weak fluorescence intensity. (D) ROS levels were quantified and expressed in bar diagram as percentage of control. (E) Cells were treated with ROS inhibitor (NAC, 2 mM) 1 h prior to CoQ₀ treatment (0–30 μM, 24 h), and cell viability of was determined by MTT assay. Results expressed as mean ± SD of three independent assays (n = 3), and significant at $*p < 0.1$; $***p < 0.001$ compared with CoQ₀ alone treated cells.

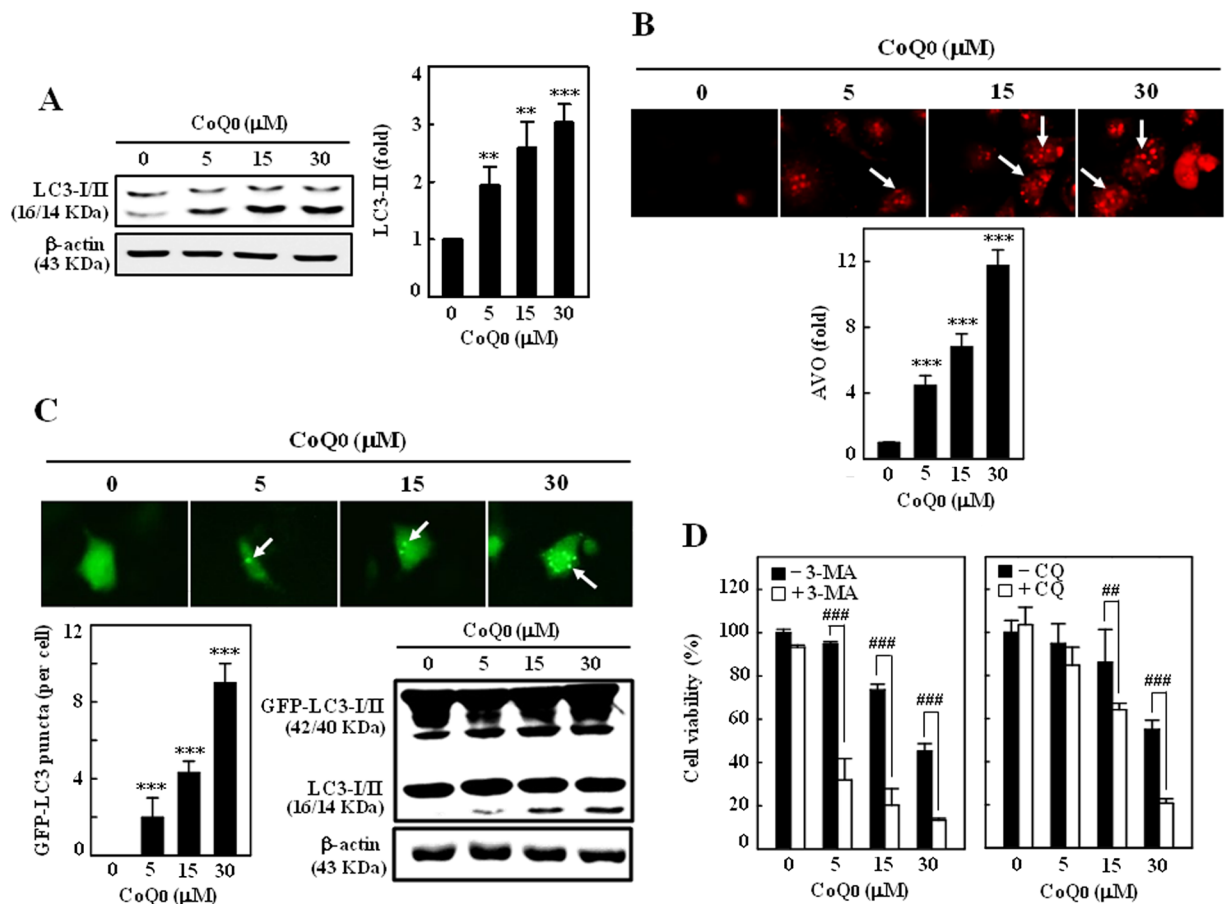


Figure 3. CoQ₀ promotes cytoprotective autophagy as a survival mechanism in SKOV-3 cells. **(A)** Cells were treated with various concentrations of CoQ₀ (0–30 μM) for 24 h and then conversion of LC3-I to LC3-II was determined by Western blot. Relative changes in the intensities of protein bands were quantified by commercially available quantitative software. **(B)** CoQ₀ induces AVOs formation. Cells were treated with CoQ₀ (0–30 μM) for 24 h and stained with AO. Formation of AVOs, represented by red fluorescence intensity (in lysosomes) was visualized under a red filter fluorescence microscope (100 × magnification). Number of AO stained cells was presented as histogram, control being as 1.0 fold. **(C)** CoQ₀ promotes conversion of GFP-LC3. Cells were transfected with GFP-LC3 expression vector for 24 h, and then treated with CoQ₀ (0–30 μM) for 24 h. GFP-LC3 dots in cells were observed under a confocal microscope (200 × magnification). Conversions of GFP-LC3 and endogenous LC3 were determined by Western blot. **(D)** Cells were treated with autophagy inhibitors (2 mM 3-MA or 10 μM CQ) for 1 h followed by CoQ₀ (0–30 μM) for 24 h, and viability was assayed by MTT assay. Results expressed as mean ± SD of three independent assays (n = 3). Significant at ***p* < 0.01; ****p* < 0.001 compared with untreated control, and significant at ##*p* < 0.01, ###*p* < 0.001 compared with CoQ₀ alone treated cells.

dose of CoQ₀ (30 μM) resulted in large number of AVOs (>10 fold) (Fig. 3B) that is corresponding to the greater accumulation of LC3-II in SKOV-3 cells.

CoQ₀ enhances GFP-LC3 conversion in SKOV-3 cells. To confirm CoQ₀-induced autophagy, GFP-LC3 plasmid was transiently transfected into the SKOV-3 cells, and conversion of GFP-LC3 and endogenous LC3 levels were monitored following CoQ₀ treatment (0–30 μM, 24 h). Images from confocal microscopy depicts that CoQ₀-treated cells represented by a cornucopia of green LC3 punctate dots in the cytoplasm, while the control cells showed a diffused and weak LC3 punctate dots (Fig. 3C). We demonstrated that CoQ₀ increased both the percentage of cells with GFP-LC3 dots and the average numbers of GFP-LC3 dots per cell in a dose-dependent fashion (Fig. 3C). Western blot results further convinced that CoQ₀ treatment significantly promoted the conversion of LC3-1 to LC3-II in SKOV-3 cells (Fig. 3C).

CoQ₀ activates autophagy as a survival mechanism in SKOV-3 cells. Autophagy has been claimed to play a paradoxical role in controlling of cell death and survival in response to various stimuli³⁴. Since CoQ₀ shown to activate autophagy in SKOV-3 cells, we wonder whether this autophagy could contribute to cell death or survival. To disclose this phenomenon, SKOV-3 cells were pretreated with autophagy inhibitors, 3-methyladenine (3-MA, inhibitor of early autophagy/LC3-II accumulation) or chloroquine (CQ, inhibitor of late autophagy/promoter of LC3-II accumulation), and cell viability was assayed following CoQ₀ treatment (0–30 μM, 24 h).

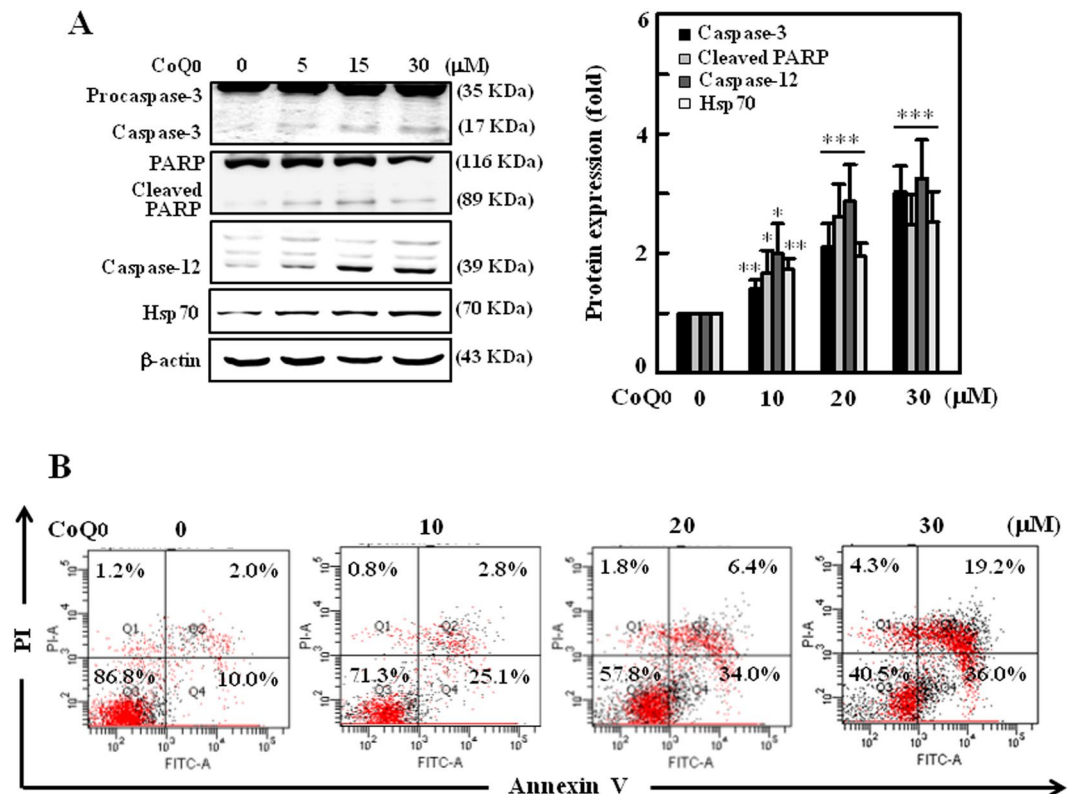


Figure 4. CoQ₀ induces apoptosis through mitochondrial and ER stress pathways in SKOV-3 cells. (A) Cells were treated with CoQ₀ (0–30 μM) for 24 h, and apoptotic proteins involved in mitochondrial pathway (procaspase-3, caspase-3 and PARP) and ER stress pathway (caspase-12 and Hsp70) were estimated by Western blot. Changes in protein intensities were quantified by commercially available software, and presented as histogram. (B) Annexin-V-FITC and PI staining was used to identify the early/late apoptosis or necrosis of cells followed by CoQ₀ (0–30 μM) treatment. Results from flow cytometry analysis in each quadrant (Q) are labeled and interpreted as follows: (Q1) PI positive, Annexin-V-FITC-negative stained cells/necrosis. (Q2) PI positive, Annexin-V-FITC-positive stained cells/late apoptosis. (Q3) cells negative for both PI and Annexin-V-FITC staining/normal live cells. (Q4) PI-negative, Annexin-V-FITC-positive stained cells/early apoptosis. Results expressed as mean ± SD of three independent assays (n = 3), and significant at **p* < 0.05; ***p* < 0.01; ****p* < 0.001 compared with untreated control cells.

Interesting results showed that inhibition of autophagy by 3-MA (2 mM) or CQ (10 μM) didn't suppress the CoQ₀-mediated cell death, instead exacerbates the cell death (Fig. 3D). These findings imply that CoQ₀-induced autophagy is not involved in death of SKOV-3 cells, which might be a cell survival mechanism.

CoQ₀ triggers apoptotic death of SKOV-3 cells via mitochondrial and ER-stress signals.

Apoptotic-cell death, a key strategic phenomenon in management of cancers is mediated by either mitochondrial or ER-stress signalling cascades^{10, 11}. To explore the patterns of apoptosis induced by CoQ₀ in SKOV-3 cells, the key molecular proteins involved in mitochondrial and ER-stress related apoptosis were determined by Western blot. As shown in Fig. 4A, procaspase-3, a highly expressed inactive form prior to CoQ₀ incubation, was dose-dependently cleaved to active caspase-3 following CoQ₀ treatment (0–30 μM, 24 h). It is known that caspase-3-mediated selective proteolytic cleavage of poly (ADP-ribose) polymerase (PARP) is a hallmark of apoptosis³⁵. Thus, we measured the PARP levels in SKOV-3 cells, and found that CoQ₀ increased the proteolytic cleavage of 116 kDa PARP to 89 kDa fragment (Fig. 4A). Next we investigated the effect of CoQ₀ on ER-stress mediated apoptosis by detecting the changes of caspase-12 and heat shock protein-70 (HSP-70) that are implicated in ER-stress apoptosis¹¹. We found CoQ₀ (0–30 μM) remarkably increased caspase-12 and HSP-70 expressions in a dose-dependent manner (Fig. 4A). These findings suggest that CoQ₀ activates both mitochondrial and ER-stress mediated apoptosis in SKOV-3 cells.

CoQ₀ promotes apoptosis in SKOV-3 cells.

To address whether CoQ₀ promotes apoptosis in SKOV-3 cells, next we performed Annexin-V- fluorescein isothiocyanate (FITC) and propidium iodide (PI) assay, which stain phosphatidylserine and DNA residues, respectively³⁶. The flow cytometry results showed that treatment of SKOV-3 cells with CoQ₀ (0–30 μM) dose-dependently increased the early and late apoptotic cells. The early apoptotic cells (Annexin-V-FITC-positive, PI-negative) represented in Q4 are 25.1%, 34% and 36% with 10, 20 and 30 μM CoQ₀ treatments respectively (Fig. 4B).

CoQ₀ potentiates apoptotic DNA fragmentation and inhibition of apoptosis reversed death of SKOV-3 cells. CoQ₀-induced apoptotic DNA fragmentation was determined using TUNEL assay (terminal deoxynucleotidyl transferase dUTP nick end labeling). The fluorescent microscope images revealed that CoQ₀ treatment (0–30 μM, 24 h) significantly increased the green fluorescence, TUNEL-positive cells (Fig. 5A), which denotes increased apoptotic DNA fragmentation. However, CoQ₀-induced DNA fragmentation (~6-fold, 30 μM) was significantly ($P < 0.001$) diminished in cells pretreated with caspase inhibitor, Z-VAD-FMK (benzyloxycarbonyl-valyl-alanyl-aspartyl-[O-methyl]-fluoromethylketone, 20 μM) (Fig. 5A and B). Furthermore, CoQ₀-induced PARP cleavage was also suppressed in the presence of Z-VAD-FMK, which indicates CoQ₀ activates caspase mediated apoptosis in SKOV-3 cells (Fig. 5C). To confirm that CoQ₀-induced death of SKOV-3 cell *via* activation of apoptosis, cells were pretreated with Z-VAD-FMK (20 μM, 1 h), and cell survival was assayed following CoQ₀ treatment (0–30 μM, 24 h). We found that CoQ₀-induced death of SKOV-3 cells was predominantly reversed by inhibition of apoptosis (Fig. 5D). These findings suggest that CoQ₀ provoked apoptotic signals contribute to death of ovarian cancer cells.

CoQ₀ increases Beclin-1/Bcl-2 and Bax/Bcl-2, and inhibits HER-2/neu/AKT/mTOR signalling in SKOV-3 cells. Since CoQ₀ reported to induce apoptosis/autophagy in SKOV-3 cells, we studied the effect of CoQ₀ (0–30 μM) on Bcl-2, and its role on Bax (pro-apoptotic) and Beclin-1 (pro-autophagic) expressions. Bcl-2 is reported to decrease the pro-autophagic property of Beclin-1, but Beclin-1 unable to neutralize the apoptotic function of Bcl-2¹⁴. In our study, we demonstrated that CoQ₀ treatment substantially decreased the Bcl-2 expression, while increased the Beclin-1 and Bax expressions in a dose-dependent fashion (Fig. 6A). Degradation of Bcl-2 probably activates apoptosis in SKOV-3 cells. The dose-dependent increase of Bax/Bcl-2 ratio with CoQ₀ represents the propagation of apoptotic mechanism in SKOV-3 cells (Fig. 6B and C).

Human epidermal growth factor receptor-2 (HER-2 *neu*) is a proto-oncogene implicated in malignant transformation, and overexpression of HER-2 has been found to aggressively promote the AKT/mTOR signals, which are responsible for regulation of tumor biology, including cancer cell invasion, differentiation and survival³⁷. We found that CoQ₀ treatment (30 μM, 0–24 h) downregulated the phosphorylated HER-2 (Y1221) levels. This decrease was accompanied with substantial time-dependent loss of p-AKT (Ser473) and p-mTOR (S2448) levels (Fig. 6D). CoQ₀ enhanced the proteolytic cleavage of PARP (116 KDa to 89 KDa), which supports activated apoptotic signals in cancer cells (Fig. 6D). These results explain that CoQ₀ may potentiate the apoptosis and/or autophagy mechanisms *via* suppression of HER-2/AKT/mTOR signalling cascades in SKOV-3 cells.

Inhibition of ROS production obliterates CoQ₀-induced apoptosis, but not autophagy in SKOV-3 cells. Aberrant production of ROS involved in execution of apoptosis and/or autophagy^{38, 39}. Since CoQ₀ reported to trigger the ROS production and induce apoptosis in SKOV-3 cells, we hypothesized that CoQ₀-induced ROS could propagate the apoptosis. To address this phenomenon, cells were pretreated with ROS inhibitor (NAC, 2 mM) for 1 h, and then incubated with CoQ₀ (30 μM, 24 h). We found that tremendously increased apoptotic DNA fragmentation with CoQ₀ was substantially diminished in the presence of NAC. The TUNEL positive cells with NAC are almost similar to that of control (Fig. 7A and B). CoQ₀ provoked late (31%) and early (34.7%) apoptotic-cells visualized in Q2 and Q4 were remarkably attenuated by NAC pretreatment. This was indicated by reporting only 2% (Q2) and 10.3% (Q4) of late and early apoptotic-cells following blockade of ROS production (Fig. 7C). In addition, increased proteolytic cleavage of PARP by CoQ₀ was obliterated in NAC pretreated cells (Fig. 7D and E). These results clearly demonstrating that CoQ₀-induced ROS are involved in execution of SKOV-3 cell apoptosis.

Subsequently we examined the role of CoQ₀-induced ROS on autophagy by detecting the AVOs in the presence or absence of NAC, following CoQ₀ treatment. We found fascinating results that CoQ₀-induced increased numbers of AVOs were not changed (remained same) even in the presence of NAC. This novel evidence explains that CoQ₀-induced ROS are not involved in autophagy, or autophagy is not contributing to the death of cancer cells; despite apoptosis takes place (Fig. 7F and G).

Inhibition of apoptosis suppresses CoQ₀-induced autophagy in SKOV-3 cells. Next to address the role of apoptosis on autophagy under CoQ₀ stimulation, SKOV-3 cells were treated with apoptosis inhibitor (Z-VAD-FMK, 20 μM) 1 h prior to CoQ₀ incubation (30 μM, 24 h), and changes in LC3-II accumulation, conversion of GFP-LC3 and AVOs formation were monitored. We found that increased LC3-II accumulation in CoQ₀ treated cells was noticeably limited by apoptosis inhibition (Fig. 8A). CoQ₀-induced increased AVOs were substantially decreased in Z-VAD-FMK pretreated cells (Fig. 8B and C). Subsequently, Z-VAD-FMK pretreatment to the GFP-LC3 plasmid transfected cells, significantly diminished the CoQ₀-induced conversion of GFP-LC3 and endogenous LC3 levels. This was evidenced by a dearth of green LC3 punctate dots and diffused fluorescence intensity in Z-VAD-FMK pretreated cells (Fig. 8D). CoQ₀ promoted conversion of LC3-1 to LC3-II was also impaired by apoptosis inhibitor (Fig. 8D). Our experimental evidence reveals that CoQ₀-induced apoptosis led to evoke the autophagy in SKOV-3 cells.

Inhibition of autophagy promotes apoptosis in CoQ₀-treated SKOV-3 cells. To describe whether autophagy is able to influence CoQ₀-induced apoptosis, SKOV-3 cells were pretreated with early autophagy inhibitor (3-MA, 2 mM), and occurrence of apoptotic DNA fragmentation and cleavage of PARP was measured. CoQ₀ treatment (30 μM, 24 h) increased apoptotic DNA fragmentation (~6-fold) as evidenced by increased TUNEL-positive cells. Intriguingly, 3-MA pretreatment further intensified the apoptotic DNA fragmentation in SKOV-3 cells (Fig. 9A and B). 3-MA pretreatment enhanced the proteolytic cleavage of PARP that was prominent when compared with CoQ₀ alone treatment (Fig. 9C). Evidence from our study (Fig. 3D, Fig. 9A–C) emphasizes

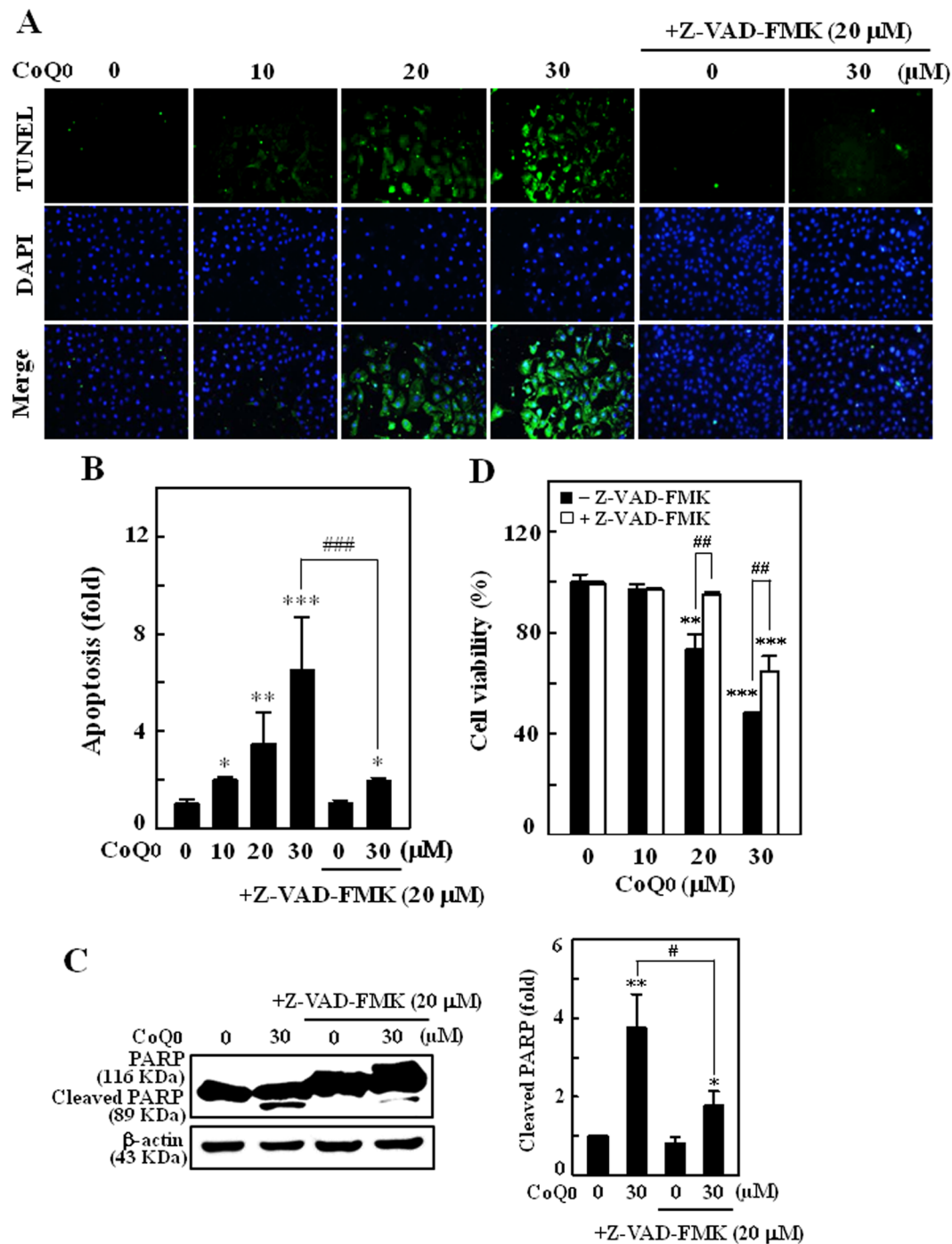


Figure 5. CoQ₀ triggers apoptotic DNA fragmentation and promote death of SKOV-3 cells. (A–D) Cells were pretreated with caspase inhibitor (Z-VAD-FMK, 20 μM) for 1 h followed by CoQ₀ (0–30 μM) for 24 h. (A) Apoptotic DNA fragmentation was determined by TUNEL assay. The green fluorescence indicates TUNEL-positive cells in the microscopic fields (200 × magnification) from three separate samples. (B) The fold of apoptotic cells was calculated by quantifying the fluorescence intensity using commercially available software. (C) Cleavage of PARP was estimated by Western blot. Changes in protein intensities were quantified by commercially available software. (D) Cell viability with or without Z-VAD-FMK treatment was determined by MTT assay. Values expressed as mean ± SD of three independent assays (n = 3). Significant at **p* < 0.05; ***p* < 0.01; ****p* < 0.001 compared with untreated control, and significant at ##*p* < 0.01; ###*p* < 0.001 compared with CoQ₀ alone treated cells.

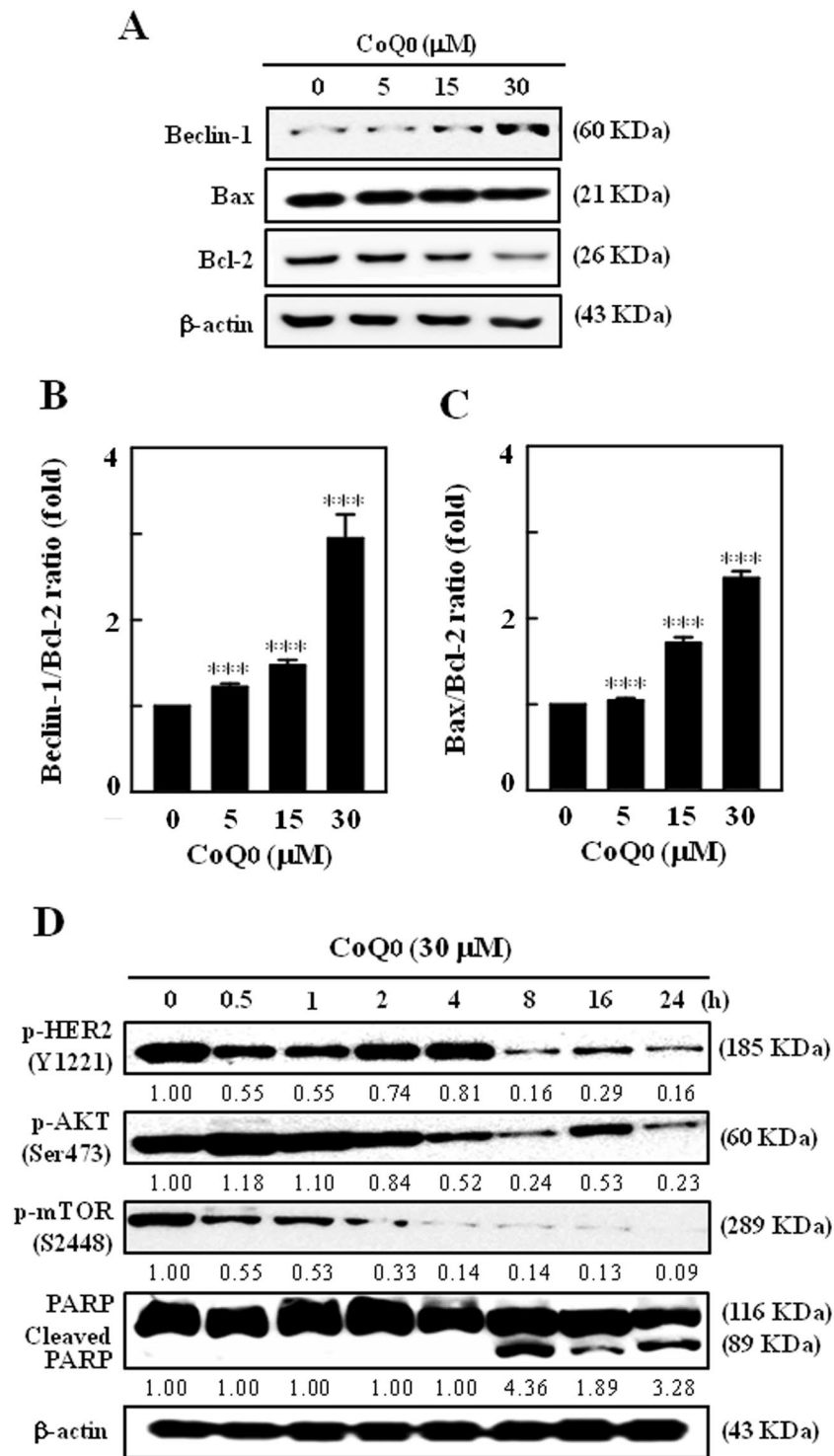


Figure 6. CoQ₀ increases Beclin-1/Bcl-2 and Bax/Bcl-2 ratios, and inhibits HER-2/*neu*/AKT/mTOR signalling in SKOV-3 cells. **(A)** Dose-dependent effect of CoQ₀ (0–30 μM, 24 h) on changes in Beclin-1, Bax and Bcl-2 proteins were determined by Western blot. Relative changes in the ratio of **(B)** Beclin-1/Bcl-2 and **(C)** Bax/Bcl-2 in accordance to dose were quantified by commercially available software, and presented as a histogram, control representing as 1.0 fold. Results expressed as mean ± SD of three independent assays (n = 3), and significant at ****p* < 0.001 compared with untreated control cells. **(D)** Time-dependent effect of CoQ₀ (0–24 h, 30 μM) on phosphorylation of HER-2/*neu* (Y1221), AKT (Ser473) and mTOR (S2448), and cleavage of PARP were determined by Western blot. Results expressed as mean ± SD of two independent assays (n = 2).

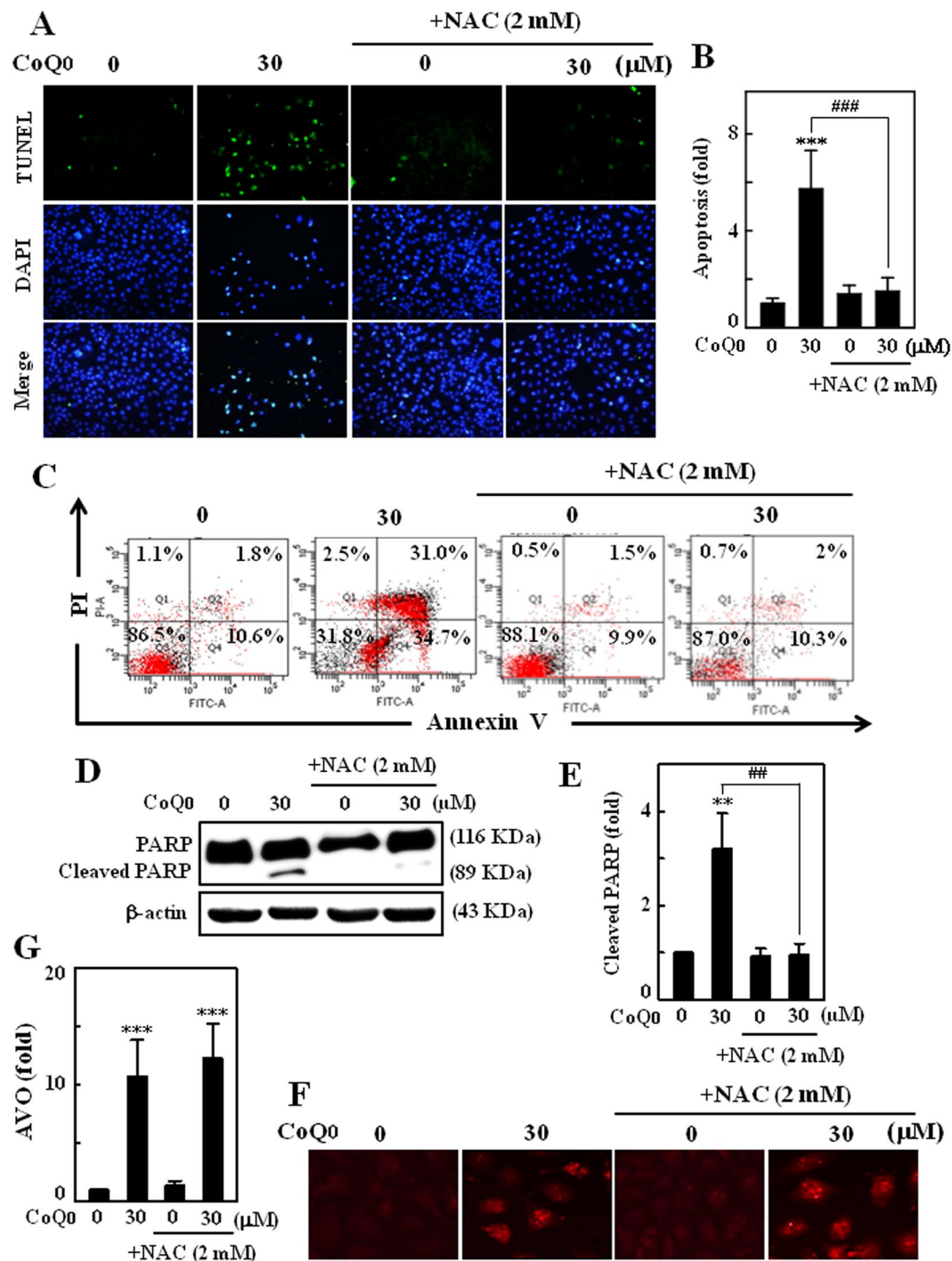


Figure 7. CoQ₀-induced ROS involved in induction of SKOV-3 apoptosis, but not autophagy. (A–G) Cells were pretreated with NAC (2 mM) for 1 h, and then incubated with CoQ₀ (30 μM) for 24 h. (A) Induction of apoptosis (DNA fragmentation) was determined by TUNEL assay in the presence or absence of NAC. The green fluorescence indicates TUNEL-positive cells in microscopic fields (200 × magnification). (B) The fold of apoptotic cells was calculated by measuring the fluorescence intensity using commercially available software. (C) Annexin-V-FITC and PI staining was used to identify the early/late apoptosis or necrosis of SKOV-3 cells. (D) Cleavage of PARP was monitored by Western blot. (E) Changes in protein intensities were quantified using commercially available software. (F) Formation of AVOs was visualized under a red filter fluorescence microscope (100 × magnification) using AO stain. (G) Number of AO stained cells with CoQ₀ or NAC was presented as histogram, control being as 1.0 fold. Results expressed as mean ± SD of three independent assays (n = 3). Significant at ***p* < 0.01; ****p* < 0.001 compared with untreated control, and significant at ##*p* < 0.01; ###*p* < 0.001 compared with CoQ₀ alone treated cells.

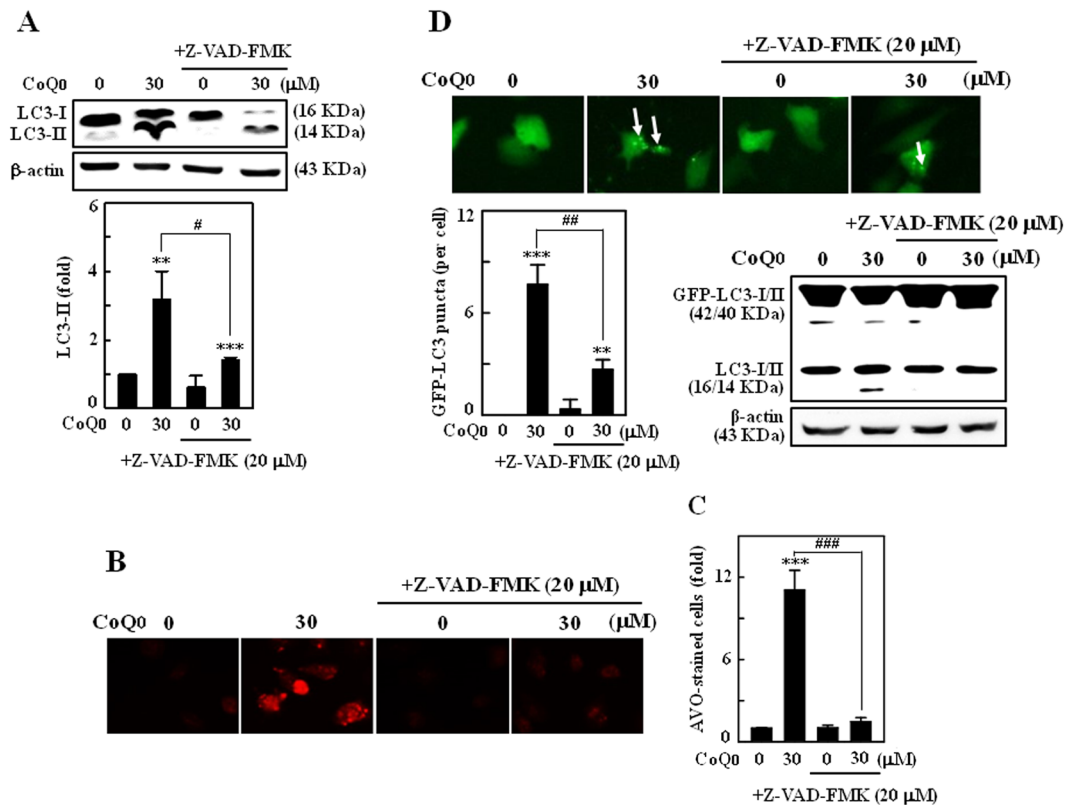


Figure 8. Inhibition of apoptosis suppressed CoQ₀-induced autophagy in SKOV-3 cells. (A–C) Cells were pretreated with caspase inhibitor (Z-VAD-FMK, 20 μM) for 1 h, and then incubated with CoQ₀ (30 μM) for 24 h. (A) LC3-I/II was determined using Western blot, and relative changes in protein intensities were quantified using commercially available software. (B) Formation of AVOs was visualized under a red filter fluorescence microscope (100 × magnification) using AO stain. (C) Number of AO stained cells with CoQ₀ or Z-VAD-FMK treatment was presented as histogram, control being as 1.0 fold. (D) Cells were transfected with GFP-LC3 expression vector for 24 h before Z-VAD-FMK and CoQ₀ treatment. GFP-LC3 dots in cells were observed under a confocal microscope (200 × magnification). Conversions of GFP-LC3 and endogenous LC3 were determined by Western blot. Results expressed as mean ± SD of three independent assays (n = 3). Significant at ***p* < 0.01; ****p* < 0.001 compared with untreated control, and significant at #*p* < 0.05; ##*p* < 0.01; ###*p* < 0.001 compared with CoQ₀ alone treated cells.

that induction of cytoprotective autophagy may renders to delay or suppress the onset of CoQ₀-induced apoptosis or SKOV-3 cell death.

CoQ₀ suppresses tumor growth in SKOV-3 xenografted nude mice. To examine the *in vivo* anti-tumor activity of CoQ₀, we used nude mice and ovarian cancer SKOV-3 cells were subcutaneously xenografted into the mice, and then treated with CoQ₀ (1.5 and 2.5 mg/kg) or vehicle for 52 days. During the experimental period no significant body weight loss was noticed among the groups, and all mice appeared healthy (Fig. 10A). Besides, no signs of the adverse effects or toxicity of CoQ₀ was observed in nude mice, according to microscopic examination of individual organs (data not shown). The tumor volume was measured for every 4 days until 52 days, and found that both doses of CoQ₀ (1.5 and 2.5 mg/kg) inhibited the tumor volume, higher dose being more effective in a time-course (Fig. 10B). Next, to assess CoQ₀ effect on tumor weight, all mice including control were photographed, and excised xenografted tumor tissues were weighed. Consistent to the tumor volume, tumor weight was also considerably decreased with CoQ₀ compared with control mice (Fig. 10C). These results revealed that CoQ₀ suppressed the tumor growth in SKOV-3 xenografted nude mice.

CoQ₀ inhibits mitosis and promotes apoptosis in tumors of SKOV-3 xenografted mice. To delineate the reason why CoQ₀ suppressed the tumor size and weight, we performed histopathological and TUNEL assays to examine the mitosis and apoptosis in tumor tissues. Microscopic images illustrated that the control tumor cells were large in size, round to oval in shape with predominant nucleoli. Tumor cells expressed high levels of cellular activity and mitotic figures, indicating proliferating cells. However, tumor sections of CoQ₀-treated mice (1.5 and 2.5 mg/kg) showed smaller cells with shrunken, condensed and pyknotic nuclei, which indicates inactivity or regression of tumor cells (Fig. 11A). The quantified mitotic-positive cells that were abundant in control tumors were notably inhibited following CoQ₀ treatment (Fig. 11B). Conversely, CoQ₀ significantly promoted the apoptosis in tumors of xenografted mice (Fig. 11A and B), which was confirmed by

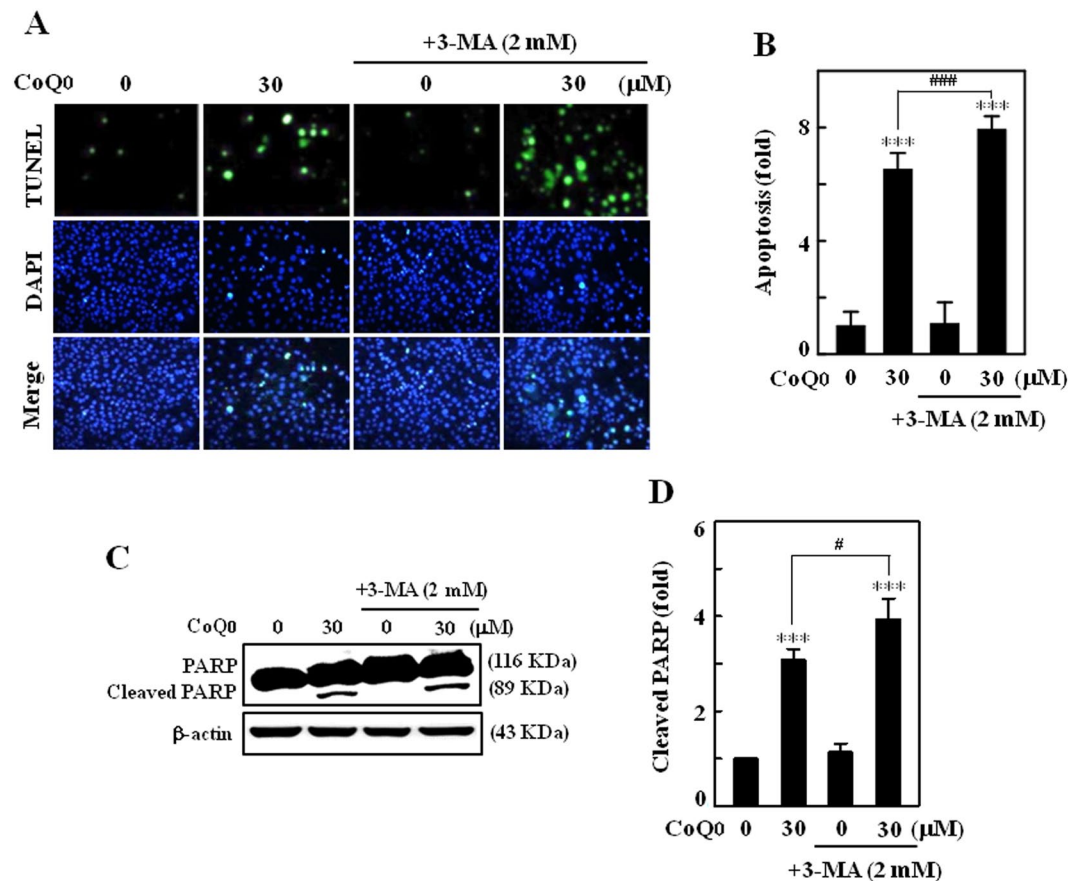


Figure 9. Inhibition of autophagy potentiated CoQ₀-induced apoptosis in SKOV-3 cells. (A–D) Cells were pretreated with autophagy inhibitor (3-MA, 2 mM) for 1 h, and then incubated with CoQ₀ (30 μM) for 24 h. (A) Induction of apoptosis (DNA fragmentation) was determined by TUNEL assay in the presence or absence of 3-MA. The green fluorescence indicates TUNEL-positive cells in microscopic fields (200 × magnification). (B) The fold of apoptotic cells was calculated by measuring the fluorescence intensity using commercially available software. (C) Cleavage of PARP with or without 3-MA pretreatment was determined by Western blot. (D) Changes in protein intensities were quantified using commercially available software. Results expressed as mean ± SD of three independent assays (n = 3). Significant at ****p* < 0.001 compared with untreated control, and significant at **p* < 0.05; ****p* < 0.001 compared with CoQ₀ alone treated cells.

a dose-dependent increase of apoptotic DNA fragmentation. Results from TUNEL assay showed CoQ₀ treatment enhanced the TUNEL-positive cells compared with vehicle (Fig. 11C and D). Our evidence confirmed that the anti-tumor activity of CoQ₀ in xenografted tumors is associated with decreased proliferation and increased apoptosis.

Discussion

Owing to its potent anticancer/cytotoxic properties against human breast cancer²⁵, and lung cancer cells⁴⁰, we assume that CoQ₀ could be a potential candidate to treat human ovarian carcinoma cells. For the first time, we have demonstrated that CoQ₀, isolated from *Antrodia camphorata*, potently killed the ovarian SKOV-3 cancer cells and induced cell-cycle arrest *via* decreased cell-cycle regulatory proteins. CoQ₀ triggered the intracellular ROS production, which then contributed to activate and propagate apoptotic signals. CoQ₀-induced apoptosis was evidenced by increased apoptotic DNA fragmentation, higher number of early/late apoptotic cells and dysregulated Bax/Bcl-2 ratio. Both mitochondrial and ER-stress mediated apoptotic signals are implicated in execution of apoptosis. The blockade of ROS production by NAC treatment diminished pro-apoptotic signals and cell death. On the other hand, activation of autophagy by CoQ₀ was evidenced by increased LC3-II accumulation, GFP-LC-3 punctuated patterns and AVOs appearance, however not contributed for autophagic-cell death. Inhibition of apoptosis by Z-VAD-FMK reversed CoQ₀-induced autophagy, while inhibition of autophagy by 3-MA/CQ exaggerated CoQ₀-induced apoptotic signals. These findings explain that CoQ₀-induced apoptosis evokes cytoprotective autophagy, which may counteract the CoQ₀-induced pro-apoptotic signals and hinder the CoQ₀ anticancer properties. Furthermore, CoQ₀ treatment to SKOV-3 xenografted nude mice suppressed the tumor volume. Xenografted tumors after CoQ₀ treatment represented by significantly decreased mitotic-cells and tremendously increased apoptotic-cells and DNA fragmentation. Taken together, our findings revealed that CoQ₀ displays both *in vitro* and *in vivo* antitumor properties. CoQ₀-induced ROS-mediate the apoptosis and activates cytoprotective/survival autophagy in human ovarian cancer cells.

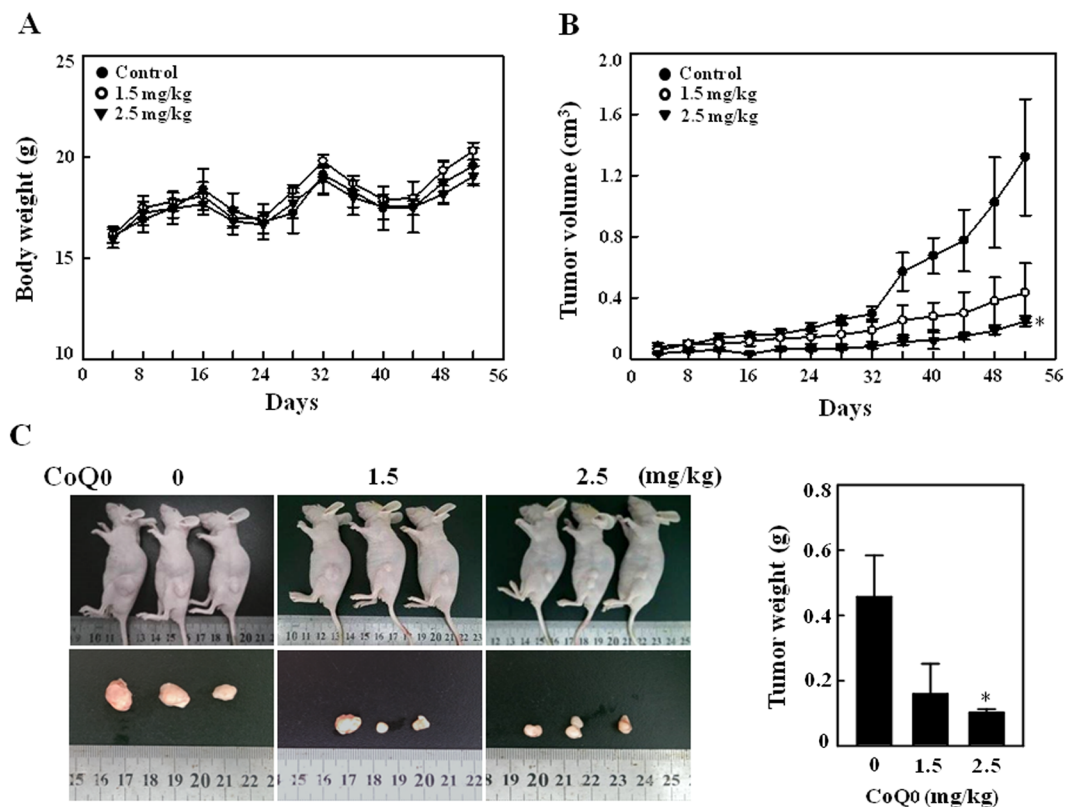


Figure 10. CoQ₀ inhibits tumor growth in SKOV-3 xenografted nude mice. (A–C) Time-course effect of CoQ₀ on growth of SKOV-3 xenografted nude mice was evaluated. Ovarian cancer cells (3×10^6 cells) were subcutaneously implanted into the flanks of nude mice on day 0 and inoculated for 7 days. Mice were subsequently treated with CoQ₀ (1.5 and 2.5 mg/kg) or vehicle (control) on every 4 days for 52 days. Changes in bodyweight (A) and tumor volume (B) were recorded for every 4 days, until 52 days. (C) On day 52, animals were photographed, and excised tumor tissue was weighed. Results expressed as mean \pm SD of three independent assays ($n = 3$). Significant at * $p < 0.05$; compared with vehicle treated mice.

Induction of apoptosis/autophagy, inhibition of cell survival and/or cell-cycle arrest by chemical substances or biological agents are the principal strategies in treatment of a variety of cancers, including ovarian carcinoma^{19,27,41}. In this study, we demonstrated that CoQ₀ treatment to ovarian cancer SKOV-3 cells produced potent cytotoxic effects, as indicated by a profound increase of cell death and aberrant morphological changes. Previous study reported that among several methoxy-substituted cyclic compounds, CoQ₀ is the strongest cytotoxic analog that inhibited the growth of MDA-MB-231 and SKBr3 human breast cancer cells. The cytotoxicity of CoQ₀ was associated with increased proportion of cells undergoing apoptosis, and this phenomenon was addressed by the induction of G₀/G₁ cell-cycle arrest in MDA-MB-231 cells and S-phase arrest in SKBr3 cells²⁵. CoQ₀ isolated from *Antrodia cinnamomea* submerged cultures has also reported to possess anticancer property by the decreased viability of A549, HepG2 and SW480 cancer cells, and increased ROS-mediated apoptosis⁴⁰.

Previously, we have shown that treatment of SKOV-3 cells with fermented culture broth of *Antrodia camphorata* inhibited the proliferation, and caused G₂/M cell-cycle arrest through the downregulation of cyclin D1, cyclin A and CDK1, and upregulation of p27 expressions²⁷. The CoQ₀ used in this study is a novel quinone derivative of *Antrodia camphorata*, which contain zero isoprenoid side chains. CoQ₀-induced death of SKOV-3 cells in this study was also accompanied by the G₂/M-phase cell-cycle arrest and decreased cell-cycle regulatory proteins (cyclin B1, CDK1, cyclin A and CDK2). Since overexpression of CDKs activity is often the cause of human cancer, their function is tightly regulated by cell-cycle inhibitors, such as the p21 and p27 Cip/Kip proteins. It has been stated that following anti-mitogenic signals or DNA damage, the proteins, p21 and p27 can bind to cyclin-CDK complexes to inhibit their catalytic activity and induce cell-cycle arrest⁴². In our study, the anti-mitogenic signals and apoptotic DNA damaging actions of CoQ₀ perhaps activates p21 and p27 expressions, which then bind to cyclin-CDK complex to inhibit their expression in SKOV2 cells. Thus, suppression of cell-cycle promoting proteins and induction of cell-cycle arrest by CoQ₀ may contribute to inhibit the ovarian cancer cell survival.

Aberrant production of ROS by oxidants or chemical substances play an important role in execution of apoptosis by activating the pro-apoptotic signals^{33,38}. Here we found that profoundly increased ROS production with CoQ₀ was accompanied by an increased death of SKOV-3 cells, and blockade of ROS production by NAC treatment substantially diminished the CoQ₀-induced cell death. Coenzyme Q exists in biomembranes act as an electron carrier and reversibly changes to either oxidized (CoQ), intermediate (CoQ^{•-}) or reduced (CoQH₂) form²⁴. During conversion from one form to another, short chain CoQ^{•-} comes into contact with cytoplasm,

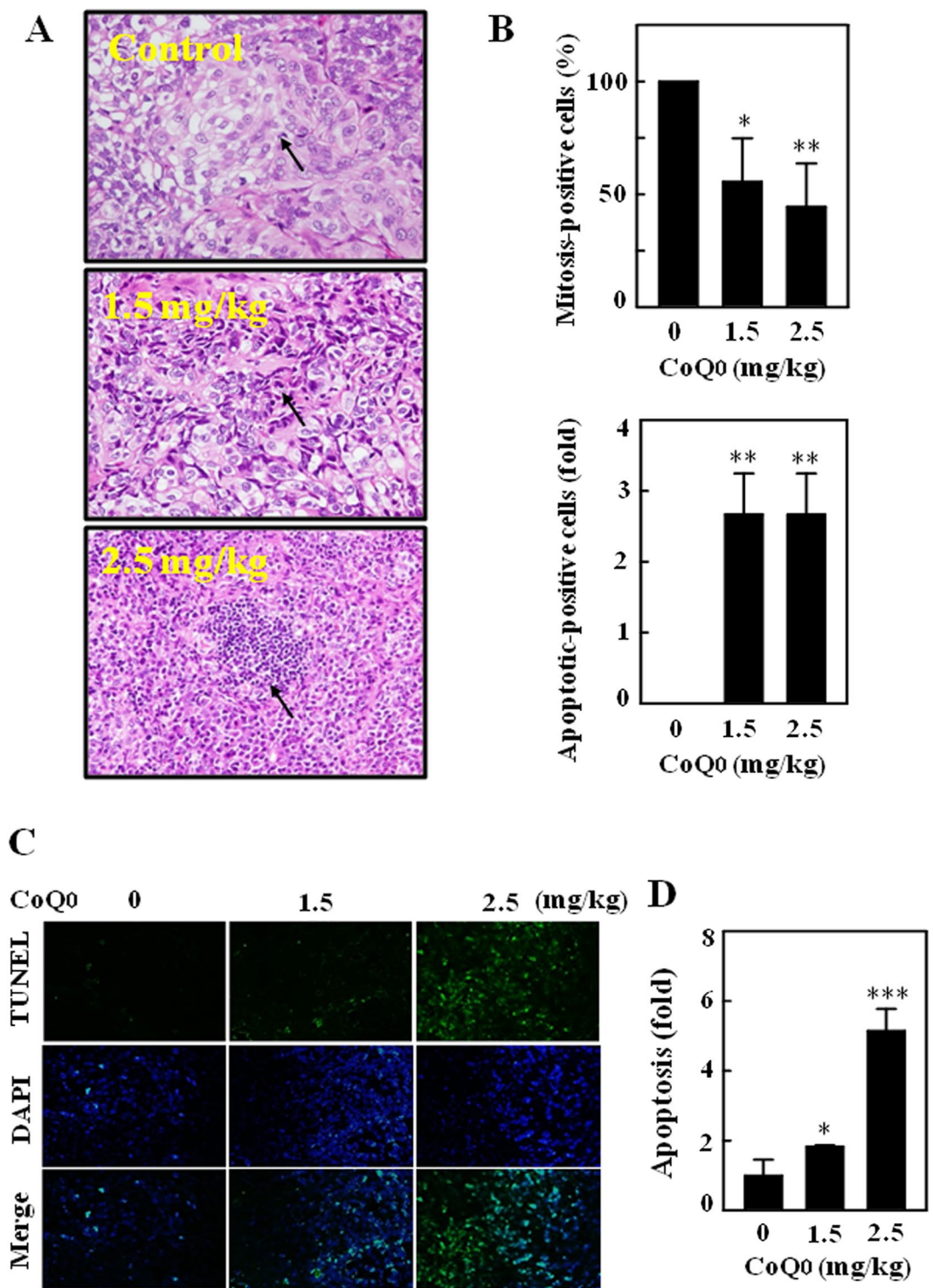


Figure 11. Histopathological analyses of mitosis and apoptosis in the tumors of SKOV-3 xenografted nude mice followed by CoQ₀ treatment. (A,B) Histopathological staining was performed to detect the mitotic- and apoptotic-cells in SKOV-3 xenografted tumors following CoQ₀ (1.5 and 2.5 mg/kg) treatment using light microscopy (20 × and 200 × magnification). Arrows indicate mitotic (tumor control) and pyknotic tumor cells (CoQ₀). The number of mitotic-positive and apoptotic-positive cells in microscopic fields of 3 samples was averaged, and presented as histogram. (C,D) *In situ* detection of apoptosis was performed using TUNEL staining in tumor sections from control and experimental analogues treated with CoQ₀ (1.5 and 2.5 mg/kg). The number of TUNEL-positive cells were quantified from 3 microscopic fields, and averaged. Results expressed as mean ± SD of three independent assays (n = 3). Significant at * $p < 0.05$; ** $p < 0.01$; *** $p < 0.001$ compared with vehicle treated mice.

auto-oxidation with O₂ occurs and generates ROS⁴³. Doughan *et al.*, demonstrated that mitoquinone (MitoQ) may be the pro-oxidant and pro-apoptotic, because its quinone group can participate in redox cycling and superoxide radical production. MitoQ-induced ROS production appears to stimulate the activity of caspase-3 and endothelial cell apoptosis⁸. Ubiquinone 0 (Ub₀) also known as CoQ₀ reported to dramatic increase of ROS production in culture rat liver Clone-9 cells, which is prominent than the other analogs (Ub₅ and Ub₁₀). Particularly, Ub₀ induced PTP opening in cancerous rat liver MH1C1 cells, and promoted PTP-dependent cell death²³. Indeed, ROS accumulation can cause depolarization of mitochondrial membrane and results in increased release of mitochondrial proteins, including apoptosis-inducing factor (AIF) that certainly promote apoptosis^{44,45}. A study on human lung carcinoma cells showed that sodium selenite induced ROS-mediated intrinsic apoptosis and mitochondrial dysfunction was blocked by ROS inhibition³³. Another recent study reported that CoQ₀ provoked the ROS-mediated apoptosis of lung cancer cells, and increased apoptotic cells were noticeably inhibited with antioxidant pretreatment⁴⁰. These results elucidate that the intracellular ROS are critically involved in the propagation of apoptosis in SKOV-3 cells.

In line with this, we demonstrated that CoQ₀-induced apoptotic DNA fragmentation, PARP cleavage and early/late apoptosis were substantially reversed *via* ROS inhibition in SKOV-3 cells. CoQ₀-induced ROS-mediated apoptosis appears to be executed by mitochondrial- and ER stress-dependent signalling cascades. It has been described that the cleavage of procaspase-3 into active caspase-3 proceeds to fragmentation of PARP, and culminating the death of cell^{10,12}. PARP, an important nuclear enzyme involved in DNA repair is a substrate for activated caspase-3, and fragmentation of PARP is considered a hallmark of mitochondrial apoptosis¹³. Cleavage of procaspase-3 is an early event in apoptosis induced by chemotherapeutic agents, and activated caspase-3 also promotes DNA fragmentation⁴⁶. Here, we found the marked increase of caspase-3 and PARP fragmentation in CoQ₀-treated cells. Interestingly, pharmacological inhibition of caspase activation by Z-VAD-FMK or blockade of ROS production by NAC resulted in a diminution of CoQ₀-induced PARP fragmentation followed by a suppressed cell death. These findings support the occurrence of mitochondrial apoptosis in CoQ₀-treated ovarian cancer cells. In fact, mitochondrial apoptosis is known to be stimulated by a wide range of cellular stresses, including overwhelming production of ROS, DNA damage and cytoskeletal disruption^{12,38}. CoQ₀-induced mitochondrial apoptosis was further addressed by the increased production of intracellular ROS levels and apoptotic DNA fragmentation in SKOV-3 cells.

ER stress, represented by an increased accumulation of unfolded proteins due to multiple stimuli, including oxidants, triggers a conserved series of signals to ameliorate the accumulation of unfolded proteins. However, if these signalling events are severe or protracted, they can induce cell death¹¹. ER molecular chaperone, HSP70 and caspase-12 are said to be involved in the ER stress-specific apoptosis^{11,47}. We found increased expressions of caspase-12 and HSP-70 proteins in cells incubated with CoQ₀, which implies the activation of ER stress-mediated apoptosis. Caspase-12 is predominantly localized to the ER, and specifically activated by the apoptotic signals with an ER stress component⁴⁷. The bile salt sodium deoxycholate, an apoptosis inducer was found to activate the HSP-70 in liver cells along with other genes involved in ER stress and DNA damage. This study suggested that activated chaperone protein HSP-70 may be an additional stress response due to malfunctioning of proteins in ER⁴⁸.

Our findings further demonstrated that CoQ₀ induced early/late apoptotic death of SKOV-3 cells. Along with aberrant morphological changes, results from Annexin-V/PI assay showed the greater number of early (Annexin-V^{+ve}/PI^{-ve}) and late (Annexin-V^{+ve}/PI^{+ve}) apoptotic cells following CoQ₀ treatment. However, this phenomenon was not observed in NAC pretreated cells, which indicates the involvement of ROS in apoptosis. Treatment of HL60 cells with different CoQ structures (CoQ₁, CoQ₂ and CoQ₄) reported to inhibit the proliferation, initial S-phase arrest followed by G₀/G₁-phase cell-cycle arrest at later time points, and induction of apoptosis⁴⁹. A recent study by Chung and colleagues showed that CoQ₀ enhanced both early and late apoptosis in human lung cancer cells, and antioxidant pretreatment diminished the apoptotic-cell death⁴⁰. Several studies demonstrated that quinones or certain methoxy-containing analogs of CoQ with structural similarities to CoQ₀ are able to produce cytotoxic effects on human cancer cells by the induction of apoptosis^{24,49}. A study carried-out using different CoQ analogs reported the increased apoptosis, DNA fragmentation and caspase-3 activation with CoQ₂ and CoQ₄, but not with CoQ₆ or CoQ₁₀ in HL60 human leukemia cells⁴⁹. These findings imply that the anticancer or pro-apoptotic properties of CoQ analogs may be varied based on the length of isoprenyl side chain, and position of the methoxy-substitutions on the quinone nucleus. Irrespective of cell lines, CoQ₀ that contains zero isoprenoid units inhibit ovarian cancer cell growth and induce early/late apoptosis through the ROS signals.

On the other hand, emerging evidence shows that autophagy constitutes a potential target for cancer therapy, and induction of autophagy in response to therapeutics can be viewed as a cell-death or cell-survival phenomenon that contributes to the anticancer efficacy¹⁹. For the first time, we demonstrated the novel function of CoQ₀, that is induction of autophagy in the ovarian cancer cells. This phenomenon was evidenced by the increased conversion of LC3-I to LC3-II (membrane bound), multiplied AVOs formation and elevated Beclin-1 expression following CoQ₀ treatment. Induction of autophagy by CoQ₀ was further confirmed by the confocal images illustrating the abundance of green GFP-LC3 puncta. The increased appearance of AVOs, a hallmark of autophagy is associated with the increased accumulation of lipidated LC3 in cells¹⁵. CoQ₀-induced higher numbers of AVOs and corresponding increased distribution of GFP-LC3-II punctates in SKOV-3 cells are explaining the recruitment of LC3-II to autophagosomes. Antroquinonol, a ubiquinone derivative of *Antrodia camphorata* has been reported to increase the LC3-II accumulation and a certain degree of autophagic-death of pancreatic carcinoma cells³⁰. Since mTOR signalling is considered a key negative regulator of autophagy⁵⁰, we determined the CoQ₀ effect on phosphorylated mTOR levels, and found severely inhibited p-mTOR (S2448) levels in SKOV-3 cells. This was accompanied by a simultaneous decrease of p-AKT levels and increase of Beclin-1/Bcl-2 ratio, which denotes activation of autophagy in SKOV-3 cells. It has been claimed that excessive production of ROS can act as intracellular messengers to trigger autophagy³⁹. To address whether CoQ₀-induced ROS involved in activation of autophagy in SKOV-3 cells, we detected the AVOs formation in the presence and absence of NAC. It is interesting

to note that inhibition of ROS production by NAC is unable to suppress the CoQ₀-induced AVOs formation, which indicates CoQ₀ activated autophagy is ROS-independent. Taken together, our results clearly explained that CoQ₀-induced ROS are involved in activation of the pro-apoptotic signals, but not autophagy in ovarian cancer cells.

Another most important finding of this study is that CoQ₀ activated autophagy in SKOV-3 cells didn't contribute for cell death; instead it might be a cytoprotective mechanism. There are confirmatory evidence explaining that induction of apoptotic cancer cell death by chemical substances is accompanied by a protective autophagy^{18,21,33}. Activation of autophagic pathway in response to target therapies or metabolic stress reportedly contributes to the survival of formed tumors, which might mediate resistance to the anticancer therapies^{17,51}. Of note, without addressing the role of autophagy, few studies enlightened the cytotoxicity of CoQ₀ against human lung cancer cells⁴⁰ and breast cancer cells²⁵ via induction of apoptotic-cell death. Yet it is unclear, whether CoQ₀-induced autophagy contributes to survival or death of ovarian cancer cells. First time, we demonstrated that inhibition of CoQ₀-induced autophagy by 3-MA or CQ didn't suppress the CoQ₀-induced cell death. These evidence explain that CoQ₀-induced autophagy is not involved in death of ovarian cancer cells, perhaps play a self-protective role against the cytotoxic effects of CoQ₀. However, it can't be ruled out that activation of autophagy by anticancer drugs/oxidants act as an alternative pathway for cellular death¹⁷. Although autophagy role is controversial in cancer cells, our findings suggest that autophagy may serve as an additional target for adjuvant anticancer therapy, and inhibition of such autophagy could further strengthen the therapeutic effectiveness of CoQ₀ treatment.

The interaction between autophagy protein (Beclin-1) and anti/pro-apoptotic proteins (Bcl-2/Bcl-XL) is complex, and represents a potential important point of convergence of the apoptotic and autophagic machinery^{20,52}. It has been shown that Beclin-1 cannot neutralize the Bcl-2 function, but Bcl-2 family proteins suppress the pro-autophagic function of Beclin-1¹⁴. In our study, CoQ₀ downregulated the Bcl-2 and upregulated the Beclin-1 that indicates activation of respective apoptosis and early autophagy mechanisms in SKOV-3 cells. Similar to our studies, anticancer properties of Sulforaphane were represented by the decreased Bcl-2 levels and increased caspase-3 activation in human breast cancer cells¹⁵. Activated caspase-3 can cleave Beclin-1 protein at position 125 and 149. The truncated Beclin-1, which in turn disrupt its interaction with Bcl-2 then allows the release of pro-apoptotic molecules from the Bcl-2/Bcl-xL complex to initiate intrinsic apoptosis⁵³. In addition, caspase-mediated cleavage of Beclin-1 promote the crosstalk between apoptosis and autophagy¹⁴. CoQ₀-induced elevated Beclin-1/Bcl-2 ratio and Bax/Bcl-2 ratio in ovarian cancer cells suggest that CoQ₀ promotes cell death via pro-apoptotic signals.

HER-2/*neu* is a proto-oncoprotein belongs to the family of epidermal growth factor, overexpressed in various human cancers, including ovarian carcinoma. Overexpression of HER-2/*neu* is associated with the high risk of treatment due to highly metastatic ability of cells and resistant to drug treatments⁵⁴. We demonstrated that CoQ₀ treatment to ovarian cancer cells time-dependently inhibited the HER-2/*neu* expression. The decreased HER-2/*neu* phosphorylation was accompanied by a substantial reduction of AKT and mTOR phosphorylations. It has been shown that activation of HER-2 leads to autophosphorylation of the C-terminal tyrosines of the receptor, and implicated in regulation of cell proliferation and inhibition of apoptosis⁵⁵. Therefore, inhibition of p-HER-2 by CoQ₀ indicates decreased proliferation and increased apoptosis of SKOV-3 cells. In our previous study, we have shown that *Antrodia camphorata* that contains CoQ₀ significantly decreased the basal tyrosine kinase phosphorylation and activation of HER-2/*neu* receptors in HER-2/*neu*-overexpressed SKOV-3 cells²⁷. A recent study showed that downregulation of HER-2 by Alo-emodin in breast cancer cells resulted in decreased tumor initiation, cell migration and invasion⁹. Since overexpression of HER-2 has been linked with activation of AKT/mTOR signals that are involved in tumor biology^{27,37}, the decreased AKT/mTOR phosphorylation with CoQ₀ perhaps contributes to effective management of the ovarian cancer progression.

Apoptosis and autophagy shares the functions of several common regulators, and the crosstalk between apoptosis and autophagy decides the fate of cell in response to cellular stress³⁴. Regardless of their complex interrelationship, autophagy usually associated with cell survival, whereas apoptosis is invariably contributes to cell death^{15,56}. Accumulating evidence suggests that under certain stress circumstances, autophagy is known to act as a partner or a promoter of apoptosis. Conversely, activation of autophagy may function to prevent the onset of apoptosis, and apoptosis can also activate autophagy^{21,34,57}. It has been shown that oridonin treated L929 cells exhibited both autophagy and apoptosis, where inhibition of autophagy increased the apoptotic-cell death, which means autophagy has an anti-apoptotic function⁵⁶. Owing to the complex interactions between apoptosis and autophagy, it is necessary for careful monitoring of the key regulatory molecules to understand the cell death phenomenon induced by chemical substances. We demonstrated that CoQ₀-induced apoptosis contributes to death of ovarian cancer cells, rather than autophagy. Chemical inhibition of apoptosis diminished the CoQ₀-induced cell death by inhibition of PARP cleavage and DNA fragmentation.

Since occurrence of apoptosis always means to cell death¹², the reported autophagy in CoQ₀-treated cancer cells does not necessarily indicates autophagic-cell death. It is worth to note that inhibition of autophagy is unable to diminish the CoQ₀-induced cell death; despite intensified the apoptotic signals. On the other hand, inhibition of apoptosis is accompanied by a substantial diminution of CoQ₀-induced autophagy (decreased LC3-II accumulation and AVOs formation). Cellular stresses, such as ER-stress and mitochondrial dysfunction are reported to activate the autophagy⁵⁷. Likewise, ginsenosides F2 induces mitochondrial dysfunction and apoptotic death of breast cancer cells was accompanied by autophagy, where inhibition of autophagy enhanced the F2-induced cell death that reveals the protective role of autophagy²¹. Thus, CoQ₀-induced ER-stress and increased release of mitochondrial apoptotic proteins may be resulted in activation of the autophagy mechanism to remove the damaged organelles. These novel findings addressed that CoQ₀-induced autophagy may not participate in cell death, perhaps served as a survival mechanism against cytotoxicity and cellular stress.

To further strengthen the anticancer properties of CoQ₀, we performed the *in vivo* studies on SKOV-3 xenografted nude mice by treating with CoQ₀. We found that treatment of CoQ₀ to xenografted nude mice

significantly decreased the tumor volume. This antitumor activity appears to be associated with the inhibition of mitotic cells and a dramatic increase of apoptotic cells/DNA fragmentation in CoQ₀-treated tumors. A study by Zhang and colleagues demonstrated that treatment with EB1089, an analog of vitamin D completely suppressed the growth of tumors in ovarian cancer xenografted nude mice. In addition, fewer mitotic figures and increased TUNEL-positive apoptotic cells were also observed in the tumor sections of EB1089 treated nude mice⁵⁸. The decreased mitotic-positive cells in the tumors of *Antrodia salmonea* treated HL60 xenografted nude mice indicating the decreased cell proliferation, which may result in decreased tumor volume in nude mice⁵⁹. A recent study suggests that suppression of epithelial ovarian cancer cell invasion into the omentum by EB1089 may help to improve the survival of patients with advanced ovarian cancer³. CoQ₀ treatment to xenografted nude mice contributed to decrease the cancer cell proliferation and increased apoptosis. These *in vivo* findings confirmed the potent antitumor properties of CoQ₀ against ovarian cancer that are consistent with *in vitro* anticancer properties. Take into consideration of *in vitro* evidence, CoQ₀-induced ROS possibly involved in propagation of apoptosis in xenografted tumors.

Conclusions

For the first time, our findings demonstrated that CoQ₀ induced apoptotic-death of human ovarian cancer cells through the increased production of ROS. The blockade of ROS production by NAC suppressed CoQ₀-induced apoptotic signals and diminished cell death, but not autophagy. Chemical inhibition of apoptosis substantially retarded the CoQ₀-induced autophagy and cell death. However, inhibition of autophagy was unable to suppress the CoQ₀-induced apoptosis, instead accelerated the pro-apoptotic signals. Our experimental evidence provides insights into the complex relation between apoptosis and autophagy induced by CoQ₀ in SKOV-3 cells. We further demonstrated the *in vivo* antitumor properties of CoQ₀ in SKOV-3 xenografted nude mice. We found that CoQ₀ treatment substantially inhibited the tumor volume through decreased mitotic-cells and increased apoptotic-cells in tumors. These findings emphasize that CoQ₀ revealed potent anticancer properties through ROS-mediated apoptosis against human ovarian carcinoma cells. The inhibition of cytoprotective autophagy or further amplifying of intracellular ROS production could be the potential strategies to improve the effectiveness of cancer treatment.

Materials and Methods

Chemicals and reagents. Dulbecco's Modified Eagle's medium (DMEM), nutrient mixture F-12, fetal bovine serum (FBS), glutamine and penicillin/streptomycin were obtained from GIBCO BRL (Grand Island, NY, USA). 3-(4,5-Dimethylthiazol-2-yl)-2,5-diphenyltetrazolium bromide (MTT), *N*-acetylcysteine (NAC), *p*-iodonitrotetrazolium violet, fluorescein isothiocyanate (FITC), propidium iodide (PI), acridine orange (AO), 3-Methyladenine (3-MA), chloroquine (CQ) and 2',7'-dihydrofluorescein-diacetate (DCFH₂-DA) were purchased from Sigma-Aldrich Chemical Co. (St. Louis, MO, USA). Antibodies against cyclin B1, CDK1, cyclin A, CDK2, caspase-3, Bcl-2, Bax, and β -actin were purchased from Santa Cruz Biotechnology, Inc. (Heidelberg, Germany). Antibodies against LC3-I/II, PARP, p-HER-2/*neu*, p-AKT, p-mTOR, and Bcl-1 were obtained from Cell Signalling Technology, Inc. (Danvers, MA, USA). Antibody against GFP was purchased from Gene Tex, Inc. (Irvine, CA, USA). Antibodies against HS-70 and Caspase-12 were purchased from BD Transduction Laboratories (Hayward, CA, USA) and Millipore Corporation (Billerica, MA, USA) respectively. 4',6-Diamidino-2-phenylindole dihydrochloride (DAPI) was purchased from Calbiochem (La Jolla, CA, USA). Z-Val-Ala-Asp-fluoromethylketone (Z-VAD-FMK) was obtained from Calbiochem (San Diego, CA, USA). All other chemicals were reagent grade or HPLC grade and were supplied by either Merck & Co., Inc. (Darmstadt, Germany) or by Sigma-Aldrich.

Preparation of fermented culture broth of *Antrodia camphorata* from submerged cultures.

The *Antrodia camphorata* culture was inoculated onto potato dextrose agar and incubated at 30 °C for 15–20 days. The whole colony was subsequently added to a flask containing 50 mL sterile water. After homogenization, the fragmented mycelial suspension was used as an inoculum. The seed culture was prepared in a 20-L fermenter (BioTop Process & Equipment, Taiwan) agitated at 150 rpm with an aeration rate of 0.2 vvm at 30 °C. A five-day culture of 15 L mycelium inoculum was inoculated into a 250 L agitated fermenter (BioTop). The fermentation conditions were the same as those used for the seed fermentation, but the aeration rate was 0.075 vvm. The fermentation product was harvested at hour 331 and poured through a non-woven fabric on a 20-mesh sieve to separate the deep-red fermented culture broth and the mycelia; the culture broth was then centrifuged at 3000 × *g* for 10 min followed by passage through a 0.22- μ m filter. The culture broth was concentrated under vacuum and freeze-dried to a powder. The yield of dry matter from the culture broth was 18.4 g/L. The experiments were performed with 2–4 different batches of *Antrodia camphorata* fermented culture⁶⁰.

Isolation and characterization of CoQ₀ from *Antrodia camphorata*. The HPLC profile of the fermented culture broth of *Antrodia camphorata* was performed using a RP-18 column [COSMOSIL, 5C₁₈-AR-II, Waters, 4.6 × 250 mm] at a flow rate of 1.0 mL/min, detected at UV 254 and 220 nm. Standard solution of the fermented culture broth from *Antrodia camphorata* was prepared by dissolving it in water (5.0 mg/mL), filtered through 0.22 μ m membrane filter and applied to HPLC analysis. The mobile phase consisted of (A) acetonitrile and (B) 0.05% trifluoroacetic acid (TFA) (v/v) using a gradient elution of 5–60% A at 5–40 min. The flow rate was maintained as 1.0 mL/min and aliquots of 20 μ L were injected. According to our previous results of HPLC analysis, the amounts of CoQ₀ (Fig. 1A) in the fermented culture broth of *Antrodia camphorata* were 17.3% (254 nm) and 13.5% (220 nm), respectively⁶⁰. The purity of CoQ₀ is \geq 98%, which is similar to commercially available CoQ₀.

Cell culture and treatment. Human ovarian cancer (SKOV-3) cells were obtained from the American Type Culture Collection (ATCC, Manassas, VA, USA). Two epithelial ovarian cell lines (A2780 and CP70) were kindly provided by Dr Cheng-I Leen (National Chung Cheng University, Taiwan). Human ovarian surface epithelial (IOSE) cells were kindly provided by Dr Michael Chan (National Chung-Cheng University, Taiwan). Cells were cultured in DMEM/F12 supplemented with 10% heat-inactivated FBS, 2 mM glutamine and 1% penicillin-streptomycin-neomycin at 37 °C in a humidified incubator with 5% CO₂. Cultures were harvested and monitored for changes in cell number by counting cell suspensions using a hemocytometer (Marienfeld, Germany). Cell morphology was examined using phase contrast microscopy (200 × magnification). Cells were treated with increasing concentrations of CoQ₀ (0–40 μM), the incubation time was varied depending on the assay. Wherever applicable, cells were pretreated with various pharmacological inhibitors, including NAC (2 mM), Z-VAD-FMK (20 μM), 3-MA (2 mM) or CQ (10 μM) for 1 h, and then incubated with indicated concentration of CoQ₀ for 24 h.

Assessment of cell viability by MTT assay. The effect of CoQ₀ on viability of human ovarian carcinoma (SKOV-3, A2870 and A2870/CP-70) and human ovarian surface epithelial (IOSE) cells was determined by the MTT colorimetric assay. Briefly, cells (2.5×10^4 cells/well in 24-well plates) were treated with different concentrations of CoQ₀ (0–40 μM) for 24 h. After CoQ₀ treatment, 400 μL 0.5 mg/mL MTT in PBS was added to each well. After incubation at 37 °C for 2 h, an equal volume of DMSO (400 μL) was added to dissolve the MTT formazan crystals, and the absorbance was measured at 570 nm (A₅₇₀) using an ELISA microplate reader (μ-Quant, Winoosky, VT, USA). The percentage (%) of cell viability was calculated as: (A₅₇₀ of treated cells/A₅₇₀ of untreated cells) × 100. The assay was performed in triplicate at each concentration.

Cell-cycle analysis. Cellular DNA content was determined by flow cytometry using the propidium iodide (PI)-labeling method as described previously³¹. Briefly, cells were seeded at a density of 4×10^5 cells/dish in 10 cm dishes, and the cell-cycle was synchronized by the addition of double thymidine (3 mM) for 16 h. Cell-cycle-synchronized cells were then washed with PBS and re-stimulated to enter the G1 phase together by the addition of fresh medium, which also contained various concentrations of CoQ₀ (0–30 μM). Cells were harvested at 24 h, and the cell-cycle analysis was performed using a FAC-Scan cytometry assay kit (BD Biosciences, San Jose, CA, USA) equipped with a single argon ion laser (488 nm). The DNA content of 1×10^4 cells/analysis was monitored using the FACS Calibur system. Cell-cycle profiles were analyzed with ModFit software (Verity Software House, Topsham, ME, USA).

Protein isolation and immunoblotting. Cells (1×10^6 cells/10-cm dish) were incubated with CoQ₀ (0–30 μM) for the indicated time periods. After incubation, cells were harvested, pooled, washed once with PBS and suspended in 89 μL of lysis buffer (10 mM Tris-HCl, pH 8, 32 mM sucrose, 1% Triton X-100, 5 mM EDTA, 2 mM DTT and 1 mM phenylmethyl sulfonyl fluoride). The cell lysates were maintained on ice for 30 min and then centrifuged at 12000 rpm for 30 min at 4 °C. Total protein content was determined using Bio-Rad protein assay reagent (Bio-Rad, Hercules, CA, USA) with bovine serum albumin as a standard. The protein extracts were mixed with sample buffer (62 mM Tris-HCl, 2% SDS, 10% glycerol, and 5% β-mercaptoethanol), and the mixture was boiled at 97 °C for 5 min. Equal amounts (50 μg) of denatured protein samples were separated by 8–18% SDS-PAGE and then transferred onto polyvinylidene difluoride (PVDF) membranes overnight. The membranes were blocked with 5% non-fat dried milk in PBS containing 1% Tween-20 for 1 h at room temperature, followed by incubation with primary antibodies for overnight. The membranes were then incubated with either a horseradish peroxidase (HRP)-conjugated anti-rabbit or anti-mouse antibodies for 2 h prior to development using a Chemiluminescent substrate (Millipore, Billerica, MA, USA). The changes in protein intensities were digitized using the ImageQuant™ LAS 4000 mini (Fujifilm). Densitometric analyses were performed using commercially available quantitative software (AlphaEase, Genetic Technology Inc. Miami, FL, USA). Each assay was performed in triplicate, with control representing 1 fold, and changes in protein intensities were presented as histograms.

Measurement of intracellular ROS production. Intracellular ROS accumulation was detected by fluorescence microscopy using the cell-permeable fluorogenic probe DCFH₂-DA. Cells (2.5×10^4 cells/mL) were cultured in DMEM/F12 medium that had been supplemented with 10% FBS, and the culture medium was replaced when the cells had reached 80% confluence. To evaluate ROS generation in a time-dependent manner, the cells were treated with CoQ₀ (0–30 μM) for 0–30 min. Then culture supernatants were removed, and incubated with non-fluorescent DCFH₂-DA (10 μM) in fresh medium at 37 °C for 30 min. Intracellular ROS production was quantified by measuring the intracellular accumulation of dichlorofluorescein (DCF), which is caused by the oxidation of DCFH₂. The DCF-stained cells were captured using fluorescence microscope (200 × magnification) (Olympus, Center Valley, PA, USA). The fluorescence intensity was quantified using analysis LS 5.0 soft image solution (Olympus Imaging America Inc.,). The percentage of fluorescence intensity (ROS generation) was compared with untreated control cells, which were arbitrarily assigned a value of 100%.

Detection and quantification of acidic vesicular organelles (AVOs) formation. Formation of AVOs was detected using AO stain in SKOV3 cells treated with various concentrations of CoQ₀ (0–30 μM) for 24 h. Briefly, after designated treatments cells were washed with PBS twice, followed by staining with AO (1 μg/mL) and dilution in PBS containing 5% FBS for 15 min. After staining, cells were washed with PBS and covered with PBS containing 5% FBS. The cells were observed under a red filter fluorescence microscope and formation of AVOs in cells was visualized at 200 × magnification. AO is a lysosomotropic metachromatic and weak base membrane-permeant fluorescent dye, whose fluorescence emission is concentration dependent, from red at high concentrations (in lysosomes) to green at low concentrations (in the cytosol), with yellow as intermediate in some conditions⁶¹.

GFP-LC3 plasmid transfection and detection of GFP-LC3 dot formation in cells. LC3 cDNA was a kind gift from Dr. Jiunn- Liang Ko (Chung-Shan Medical University, Taiwan). GFP-LC3 fusion protein was used to make the autophagosomes visible in cells. The cells were seeded onto coverslips placed onto a 6-well plate (1.8×10^5 cells/well). After overnight culture, cells were transfected with 2.5 μ g GFP-LC3 expressing plasmid in each well of a 6-well plate using Lipofectamine (Invitrogen, Carlsbad, CA, USA) and incubated for 24 h. The medium was removed and fresh medium containing CoQ₀ (0–30 μ M) was added to the wells. At the end of CoQ₀ treatment (24 h), cells were washed twice with PBS, and expression of GFP-LC3 dots in cells were detected by a laser scanning confocal microscope at 200 \times magnification.

Determination of apoptotic cells by Annexin-V/PI staining. Double staining for Annexin-V-FITC and PI (propidium iodide) was performed to estimate the apoptotic rate of SKOV-3 cells. Briefly, cells were incubated with CoQ₀ (0–30 μ M) for 24 h, trypsinized, washed twice with PBS, and centrifuged at 1000 rpm for 5 min. Then, cells (1×10^6 cells/10-cm dish) were suspended in binding buffer (500 μ L) and double-stained with Annexin-V-FITC and PI for 15 min at room temperature. Then the result green (FITC) and red (PI) fluorescence of each sample was quantitatively analyzed by FACS Caliber flow cytometer (Becton Dickinson, San Jose, CA, USA) and Cell Quest software. The obtained results were interpreted as follows: (Q3) cells negative for both PI and Annexin-V-FITC staining were considered normal live cells. (Q4) PI-negative, Annexin-V-FITC-positive stained cells were considered in early apoptosis. (Q2) PI-positive, Annexin-V-FITC-positive stained cells were considered in late apoptosis. (Q1) PI-positive, Annexin-V-FITC-negative stained cells were considered in necrosis.

Apoptotic DNA fragmentation by TUNEL assay. DNA fragmentation in cells was measured using commercially available TUNEL assay kit (Calbiochem, San Diego, CA, USA). After treatment with designated inhibitors (1 h) and CoQ₀ (0–30 μ M, 24 h), apoptotic cells (2×10^4 cells/well in 8-well chamber) were harvested, fixed with 4% formaldehyde and mounted on glass slides. Apoptosis was detected by labeling the 3'-OH ends of fragmented DNA with biotin-dNTP using DNA I klenow fragment at 37 °C for 1.5 h. The slides were then incubated with horseradish peroxidase-conjugated streptavidin, followed by incubation with 3,3'-diaminobenzidine and H₂O₂. The fragmented DNA was identified by their fluorescence nuclei under a fluorescence microscope (200 \times magnification). The green fluorescence intensity was quantified using a squared section of fluorescence-stained cells with analysis LS 5.0 soft image solution (Olympus Imaging America Inc., PA, USA). The percentage of fluorescence intensity is directly proportional to the percentage of apoptotic cells, compared to untreated control cells, which were arbitrarily assigned a value of 100%.

Animals. Female athymic nude mice (BALB/*c-nu*), 5–6 weeks of age, were purchased from The National Laboratory Animal Center (Taipei, Taiwan) and were maintained in caged housing in a specifically designed pathogen-free isolation facility with a 12 h/12 h light/dark cycle. The mice had free access to rodent chow (Oriental Yeast Co Ltd., Tokyo, Japan) and water *ad libitum*. All animal experiments were strictly followed “The Guidelines for the Care and Use of Laboratory Animals” published by the Chinese Society of Animal Science, Taiwan. The entire animal study protocols were reviewed and approved by the Institutional Animal Care and Use Committee (IACUC) of China Medical University, Taichung, Taiwan.

Tumor cell inoculation and CoQ₀ treatment. A total of 9 mice were randomly divided into three groups containing three animals in each group. SKOV3 cells (3×10^6 cells, 100 μ L) were mixed in a 100 μ L matrix gel and then injected subcutaneously in a volume of 200 μ L into the right hind flanks of nude mice. The experiments were performed using cells that had been passaged fewer than 20 times. After cell inoculation for 7 days, the treatment groups received CoQ₀ (1.5 and 2.5 mg/kg b.w.) in a volume of 100 μ L *via* intraperitoneal injection every 4 days for 52 days. The control group received the vehicle (PBS) only. CoQ₀ was dissolved in PBS (containing 1% DMSO) and injections were scheduled in the morning between 10 AM and 11 AM throughout the study. To monitor drug toxicity, the body weight of each animal was measured for every 4 days. Tumor volume in mice was compared with caliper measurements of tumor length, width and depth, and then calculated every 4 days using the formula: length \times width² \times 1/2. On day 52, all mice were sacrificed and tumor tissues were removed and weighed. A veterinary pathologist examined the mouse organs, including the liver, lungs and kidneys.

Histopathological analyses. The biopsied tumor tissues were embedded in paraffin and cut into 3 mm thick sections, placed in plastic cassettes and immersed in neutral buffered formalin for 24 h. The fixed tissues were processed routinely and then embedded in paraffin, sectioned, deparaffinised, and rehydrated using standard techniques. The extent to which treatment shrunk tumor cells was evaluated by assessing the mitotic cell division in xenografted tumor sections using hematoxylin and eosin (H & E) staining for light microscopy. Then the number of mitotic cells or apoptotic cells in microscopic fields were averaged and presented as histogram. TUNEL apoptosis in the sections of CoQ₀ or vehicle treated tumors was measured using *in situ* cell death detection kit (Roche, Mannheim, Germany).

Statistical analyses. Data from *in vitro* experiments were presented as mean and standard deviation (mean \pm SD). For *in vivo* experiments, mean data values are presented with standard error (mean \pm SE). Data from both studies were analyzed using analysis of variance followed by Dunnett's test for pair-wise comparison. Statistical significance was defined as * $p < 0.05$, ** $p < 0.01$, *** $p < 0.001$ compared to untreated control cells, and significant at # $p < 0.05$; ## $p < 0.01$; ### $p < 0.001$ compared to CoQ₀ alone treated cells.

References

- Tew, W. P. Ovarian cancer in the older woman. *J. Geriatr. Oncol.* (2016).
- Yeung, T.-L. *et al.* Cellular and molecular processes in ovarian cancer metastasis. A Review in the Theme: Cell and Molecular Processes in Cancer Metastasis. *Am. J. Physiol. Cell Physiol.* **309**, C444–C456 (2015).
- Lungchukiet, P. *et al.* Suppression of epithelial ovarian cancer invasion into the omentum by $1\alpha,25$ -dihydroxyvitamin D3 and its receptor. *J. Steroid. Biochem. Mol. Biol.* **148**, 138–147 (2015).
- Benedet, J., Odicino, F. & Maisonneuve, P. FIGO (International Federation of Gynecology and Obstetrics) annual report on the results of treatment in gynecological cancer. *Int. J. Gynaecol. Obstet.* **83** (2003).
- Raja, F., Chopra, N. & Ledermann, J. Optimal first-line treatment in ovarian cancer. *Ann. Oncol.* **23**, x118–x127 (2012).
- Drisko, J. A., Chapman, J. & Hunter, V. J. The use of antioxidants with first-line chemotherapy in two cases of ovarian cancer. *J. Am. Coll. Nutr.* **22**, 118–123 (2003).
- Hseu, Y.-C. *et al.* Zerumbone attenuates TGF- β 1-mediated epithelial–mesenchymal transition via upregulated E-cadherin expression and downregulated Smad2 signalling pathways in non-small cell lung cancer (A549) cells. *J. Func Foods* **18**, 58–72 (2015).
- Doughan, A. K. & Dikalov, S. I. Mitochondrial redox cycling of mitochinone leads to superoxide production and cellular apoptosis. *Antioxid. Redox Signal.* **9**, 1825–1836 (2007).
- Ma, J. *et al.* Aloe-emodin inhibits HER-2 expression through the downregulation of Y-box binding protein-1 in HER-2-overexpressing human breast cancer cells. *Oncotarget* (2016).
- Green, D. R. Apoptotic pathways: paper wraps stone blunts scissors. *Cell* **102**, 1–4 (2000).
- Kim, I., Xu, W. & Reed, J. C. Cell death and endoplasmic reticulum stress: disease relevance and therapeutic opportunities. *Nat. Rev. Drug Discov.* **7**, 1013–1030 (2008).
- McIlwain, D. R., Berger, T. & Mak, T. W. Caspase functions in cell death and disease. *Cold Spring Harb. Perspect. Biol.* **5** (2013).
- Elumalai, P. *et al.* Induction of apoptosis in human breast cancer cells by nimbolide through extrinsic and intrinsic pathway. *Toxicol. Lett.* **215**, 131–142 (2012).
- Kang, R., Zeh, H., Lotze, M. & Tang, D. The Beclin 1 network regulates autophagy and apoptosis. *Cell Death Differ.* **18**, 571–580 (2011).
- Kanematsu, S. *et al.* Autophagy inhibition enhances sulforaphane-induced apoptosis in human breast cancer cells. *Anticancer Res.* **30**, 3381–3390 (2010).
- Kabaya, Y. *et al.* LC3, a mammalian homologue of yeast Apg8p, is localized in autophagosome membranes after processing. *EMBO J.* **19**, 5720–5728 (2000).
- Kondo, Y., Kanzawa, T., Sawaya, R. & Kondo, S. The role of autophagy in cancer development and response to therapy. *Nat. Rev. Cancer* **5**, 726–734 (2005).
- Zhang, N. *et al.* FTY720 induces necrotic cell death and autophagy in ovarian cancer cells: A protective role of autophagy. *Autophagy* **6**, 1157–1167 (2010).
- Sui, X. *et al.* Autophagy and chemotherapy resistance: a promising therapeutic target for cancer treatment. *Cell Death Dis.* **4**, e838 (2013).
- Maiuri, M. C., Zalckvar, E., Kimchi, A. & Kroemer, G. Self-eating and self-killing: crosstalk between autophagy and apoptosis. *Nat. Rev. Mol. Cell Biol.* **8**, 741–752 (2007).
- Mai, T. T. *et al.* Ginsenoside F2 induces apoptosis accompanied by protective autophagy in breast cancer stem cells. *Cancer Lett.* **321**, 144–153 (2012).
- Turunen, M., Olsson, J. & Dallner, G. Metabolism and function of coenzyme Q. *Biochim. Biophys. Acta* **1660**, 171–199 (2004).
- Devun, F. *et al.* Ubiquinone analogs: a mitochondrial permeability transition pore-dependent pathway to selective cell death. *PLoS One* **5**, e11792 (2010).
- Esaka, Y., Nagahara, Y., Hasome, Y., Nishio, R. & Ikekita, M. Coenzyme Q 2 induced p53-dependent apoptosis. *Biochim. Biophys. Acta* **1724**, 49–58 (2005).
- Somers-Edgar, T. J. & Rosengren, R. J. Coenzyme Q0 induces apoptosis and modulates the cell cycle in estrogen receptor negative breast cancer cells. *Anticancer Drugs* **20**, 33–40 (2009).
- Yang, H.-L. *et al.* Anti-angiogenic properties of coenzyme Q0 through downregulation of MMP-9/NF- κ B and upregulation of HO-1 signaling in TNF- α -activated human endothelial cells. *Biochem. Pharmacol.* **98**, 144–156 (2015).
- Yang, H.-L. *et al.* The anti-cancer activity of *Antrodia camphorata* against human ovarian carcinoma (SKOV-3) cells via modulation of HER-2/neu signaling pathway. *J. Rethnopharmacol.* **148**, 254–265 (2013).
- Hsieh, Y.-L., Wu, S.-P., Fang, L.-W. & Hwang, T.-S. Effects of *Antrodia camphorata* extracts on anti-oxidation, anti-mutagenesis and protection of DNA against hydroxyl radical damage. *BMC Complement. Altern. Med.* **15**, 1 (2015).
- Hseu, Y.-C., Chen, S.-C., Yeh, Y.-J., Wang, L. & Yang, H.-L. Antioxidant activity of *Antrodia camphorata* on free radical-induced endothelial cell damage. *J. Ethnopharmacol.* **118**, 237–245 (2008).
- Yu, C.-C. *et al.* Antroquinonol, a natural ubiquinone derivative, induces a cross talk between apoptosis, autophagy and senescence in human pancreatic carcinoma cells. *J. Nutr. Biochem.* **23**, 900–907 (2012).
- Hseu, Y.-C., Chen, S.-C., Chen, H.-C., Liao, J.-W. & Yang, H.-L. *Antrodia camphorata* inhibits proliferation of human breast cancer cells *in vitro* and *in vivo*. *Food Chem. Toxicol.* **46**, 2680–2688 (2008).
- Liu, F.-S., Yang, P.-Y., Hu, D.-N., Huang, Y.-W. & Chen, M.-J. *Antrodia camphorata* induces apoptosis and enhances the cytotoxic effect of paclitaxel in human ovarian cancer cells. *Int. J. Gynecol. Cancer* **21**, 1172–1179 (2011).
- Park, S.-H. *et al.* Induction of apoptosis and autophagy by sodium selenite in A549 human lung carcinoma cells through generation of reactive oxygen species. *Toxicol. Lett.* **212**, 252–261 (2012).
- Morselli, E. *et al.* Anti- and pro-tumor functions of autophagy. *Biochim. Biophys. Acta* **1793**, 1524–1532 (2009).
- Kaufmann, S. H., Desnoyers, S., Ottaviano, Y., Davidson, N. E. & Poirier, G. G. Specific proteolytic cleavage of poly(ADP-ribose) polymerase: An early marker of chemotherapy-induced apoptosis. *Cancer Res.* **53**, 3976–3985 (1993).
- Vermes, I., Haanen, C., Steffens-Nakken, H. & Reutelingsperger, C. A novel assay for apoptosis flow cytometric detection of phosphatidylserine expression on early apoptotic cells using fluorescein labelled annexin V. *J. Immunol. Methods* **184**, 39–51 (1995).
- Komoto, M. *et al.* HER2 overexpression correlates with survival after curative resection of pancreatic cancer. *Cancer Sci.* **100**, 1243–1247 (2009).
- Simon, H.-U., Haj-Yehia, A. & Levi-Schaffer, F. Role of reactive oxygen species (ROS) in apoptosis induction. *Apoptosis* **5**, 415–418 (2000).
- Chen, Y. & Gibson, S. B. Is mitochondrial generation of reactive oxygen species a trigger for autophagy? *Autophagy* **4**, 246–248 (2008).
- Chung, C.-H., Yeh, S.-C., Chen, C.-J. & Lee, K.-T. Coenzyme Q0 from *Antrodia cinnamomea* in submerged cultures induces reactive oxygen species-mediated apoptosis in A549 human lung cancer cells. *Evid. Based. Complement. Alternat. Med.* **2014**, 10 (2014).
- Abuharbeid, S. *et al.* Cytotoxicity of the novel anti-cancer drug rViscumin depends on HER-2 levels in SKOV-3 cells. *Biochem. Biophys. Res. Commun.* **321**, 403–412 (2004).
- Coqueret, O. New roles for p21 and p27 cell-cycle inhibitors: a function for each cell compartment? *Trends Cell Biol.* **13**, 65–70 (2003).
- Jemiota Rzezińska, M., Latowski, D. & Strzałka, K. Incorporation of plastoquinone and ubiquinone into liposome membranes studied by HPLC analysis.: The effect of side chain length and redox state of quinone. *Chem. Phys. Lipids* **110**, 85–94 (2001).

44. Reed, J. C. Mechanisms of Apoptosis. *Am. J. Pathol.* **157**, 1415–1430 (2000).
45. Liu, P.-L., Chen, Y.-L., Chen, Y.-H., Lin, S.-J. & Kou, Y. R. Wood smoke extract induces oxidative stress-mediated caspase-independent apoptosis in human lung endothelial cells: role of AIF and EndoG. *Am. J. Physiol. Lung Cell Mol. Physiol.* **289**, L739–L749 (2005).
46. Yang, X. *et al.* Resistance to chemotherapy-induced apoptosis via decreased caspase-3 activity and overexpression of antiapoptotic proteins in ovarian cancer. *J. Cancer Res. Clin. Oncol.* **130**, 423–428 (2004).
47. Nakagawa, T. *et al.* Caspase-12 mediates endoplasmic-reticulum-specific apoptosis and cytotoxicity by amyloid- β . *Nature* **403**, 98–103 (2000).
48. Bernstein, H. *et al.* Activation of the promoters of genes associated with DNA damage, oxidative stress, ER stress and protein misfolding by the bile salt, deoxycholate. *Toxicol. Lett.* **108**, 37–46 (1999).
49. Yonezawa, Y. *et al.* Inhibitory effect of coenzyme Q1 on eukaryotic DNA polymerase γ and DNA topoisomerase II activities on the growth of a human cancer cell line. *Cancer Sci.* **97**, 716–723 (2006).
50. Liang, C. Negative regulation of autophagy. *Cell Death Differ.* **17**, 1807–1815 (2010).
51. Janku, F., McConkey, D. J., Hong, D. S. & Kurzrock, R. Autophagy as a target for anticancer therapy. *Nat. Rev. Clin. Oncol.* **8**, 528–539 (2011).
52. Pattingre, S. *et al.* Bcl-2 antiapoptotic proteins inhibit Beclin 1-dependent autophagy. *Cell* **122**, 927–939 (2005).
53. Czabotar, P. E., Lessene, G., Strasser, A. & Adams, J. M. Control of apoptosis by the BCL-2 protein family: implications for physiology and therapy. *Nat. Rev. Mol. Cell Biol.* **15**, 49–63 (2014).
54. Slamon, D. *et al.* Studies of the HER-2/neu proto-oncogene in human breast and ovarian cancer. *Science* **244**, 707–712 (1989).
55. Olayioye, M. A. Intracellular signaling pathways of ErbB2/HER-2 and family members. *Breast Cancer Res.* **3**, 1 (2001).
56. Cheng, Y. *et al.* Autophagy inhibits reactive oxygen species-mediated apoptosis via activating p38-nuclear factor-kappa B survival pathways in oridonin-treated murine fibrosarcoma L929 cells. *FEBS J.* **276**, 1291–1306 (2009).
57. Mizushima, N., Levine, B., Cuervo, A. M. & Klionsky, D. J. Autophagy fights disease through cellular self-digestion. *Nature* **451**, 1069–1075 (2008).
58. Zhang, X. *et al.* Growth suppression of ovarian cancer xenografts in nude mice by vitamin D analogue EB1089. *Clin. Cancer Res.* **11**, 323–328 (2005).
59. Hseu, Y.-C. *et al.* The anti-tumor activity of *Antrodia salmonea* in human promyelocytic leukemia (HL-60) cells is mediated via the induction of G1 cell-cycle arrest and apoptosis *in vitro* or *in vivo*. *J. Ethnopharmacol.* **153**, 499–510 (2014).
60. Hseu, Y.-C., Huang, H.-C. & Hsiang, C.-Y. *Antrodia camphorata* suppresses lipopolysaccharide-induced nuclear factor- κ B activation in transgenic mice evaluated by bioluminescence imaging. *Food Chem. Toxicol.* **48**, 2319–2325 (2010).
61. Boya, P. & Kroemer, G. Lysosomal membrane permeabilization in cell death. *Oncogene* **27**, 6434–6451 (2008).

Acknowledgements

This work was supported by the grants MOST-104-2320-B-039-040 -MY3, MOST-103-2320-B-039-038-MY3, NSC-103-2622-B-039-001-CC2, CMU103-ASIA -12, and CMU103-ASIA-09 from the Ministry of Science and Technology, National Science Council, Asia University and China Medical University, Taiwan. This study was supported by China Medical University under the Aim for Top University Plan of the Ministry of Education, Taiwan (CHM106-5-3).

Author Contributions

T.J.T., Y.C.H. and H.L.Y. performed the laboratory experiments and collected the data. Y.C.H., H.L.Y. and M.K. interpreted the data, drafted and revised the manuscript. J.Y.L., H.J.C., C.M.L. and Y.C.S. coordinated the study. Y.C.H. and H.L.Y. designed and supervised the study. All authors read and approved the final version of the manuscript.

Additional Information

Supplementary information accompanies this paper at doi:10.1038/s41598-017-08659-7

Competing Interests: The authors declare that they have no competing interests.

Publisher's note: Springer Nature remains neutral with regard to jurisdictional claims in published maps and institutional affiliations.



Open Access This article is licensed under a Creative Commons Attribution 4.0 International License, which permits use, sharing, adaptation, distribution and reproduction in any medium or format, as long as you give appropriate credit to the original author(s) and the source, provide a link to the Creative Commons license, and indicate if changes were made. The images or other third party material in this article are included in the article's Creative Commons license, unless indicated otherwise in a credit line to the material. If material is not included in the article's Creative Commons license and your intended use is not permitted by statutory regulation or exceeds the permitted use, you will need to obtain permission directly from the copyright holder. To view a copy of this license, visit <http://creativecommons.org/licenses/by/4.0/>.

© The Author(s) 2017